

Index for Quantifying ‘Order’ in Three-Dimensional Shapes

Takahiro Shimizu ¹, Masaya Okamoto ¹, Yuto Ieda ¹ and Takeo Kato ^{2,*} ¹ School of Integrated Design Engineering, Graduate School of Keio University, Yokohama 223-8522, Japan² Department of Mechanical Engineering, Keio University, Yokohama 223-8522, Japan

* Correspondence: kato@mech.keio.ac.jp

Abstract: In this study, we focused on assessing the symmetry of shapes and quantifying an index of ‘order’ in three-dimensional shapes using curvature, which is important in product design. Specifically, the target three-dimensional shape was divided into two segments, and the Jensen–Shannon distance was calculated for the distribution of the Casorati curvatures in both segments to determine the similarity between them. This was proposed as an indicator of the ‘order’ exhibited by the shape. To validate the effectiveness of the proposed index, sensory evaluation experiments were conducted on three shapes: extruded, rotated, and vase. For the rotated shape, the coefficient of determination between the proposed index and the sensory evaluation value of ‘order’ on a 5-point Likert scale was found to be less than 0.1. The reason for the poor correlation coefficient of determination may be attributed to the bias in human perception, where individuals tend to perceive mirror symmetry with respect to the plane that includes the vertical axis when recognizing the mirror symmetry of an object. In contrast, for the extruded and vase shapes, the coefficients of determination were 0.36 and 0.66, respectively, supporting the validity of the proposed index. Nonetheless, the coefficient of determination decreased slightly for familiar extruded shapes and asymmetric vase shapes. In future research, our aim is to quantify ‘aesthetic preference’ by combining the ‘order’ and ‘complexity’ indexes.

Keywords: aesthetics; morphological evaluation; order; symmetry; curvature



Citation: Shimizu, T.; Okamoto, M.; Ieda, Y.; Kato, T. Index for Quantifying ‘Order’ in Three-Dimensional Shapes. *Symmetry* **2024**, *16*, 381. <https://doi.org/10.3390/sym16040381>

Academic Editors: Yuanjie Shao and Changxin Gao

Received: 13 February 2024

Revised: 18 March 2024

Accepted: 19 March 2024

Published: 22 March 2024



Copyright: © 2024 by the authors. Licensee MDPI, Basel, Switzerland. This article is an open access article distributed under the terms and conditions of the Creative Commons Attribution (CC BY) license (<https://creativecommons.org/licenses/by/4.0/>).

1. Introduction

In recent years, generative design, which leverages computers for automated shape design, has gained popularity and found practical application in the design process [1–7]. An advantage of this method is its ability to design shapes that satisfy mechanical conditions such as stress and displacement [1,3]. However, the challenge lies in evaluating aspects of design aesthetics, such as ‘beauty’ or ‘preference’ (referred to as ‘aesthetic preference’), which are crucial in product design [8]. Therefore, when using this technology, designers, based on their experience and intuition, must evaluate and select the obtained shapes [9]. If a computer can quantify the shape features that designers prioritize when assessing design quality, it would be possible for a computer to conduct generative design independently, including aesthetic evaluation. This has the potential to reduce the time and cost of design processes, enabling the automated creation of high-quality shapes. Product requirements perceived by people have recently started changing from largely functional benefits (functionality and usability) to emotional benefits, including an “aesthetic liking” of product shapes [10–12]. Therefore, the use of generative design tools and methods in industry is expected to accelerate with the quantification of aesthetic preferences.

Designers typically focus on macroscopic shape attributes such as ‘complexity’, ‘order’, and ‘proportion’ when evaluating the aesthetic aspects of shapes [13–18]. Among these, complexity and order are acknowledged to influence aesthetic preferences, and quantifying these allows for the quantification of aesthetic preferences [19–24]. A summary of research related to the quantification of complexity and order in shapes is given below.

Birkhoff [20] defined complexity as the effort required to recognize an object, and numerous studies have attempted to quantify it. Birkhoff [20], Eysenck [25], Boselie [21],

and Vitz [26] characterized complexity as the number of lines in two-dimensional shapes and sought methods to quantify it. Wang et al. [27] and Saleem et al. [28] defined complexity as the dissimilarity between contour shapes when viewed from different perspectives in three-dimensional shapes. In this context, although there are studies that quantify complexity based on overall shape features such as the number of lines or contours, Farin et al. [29] suggested that designers frequently focus on subtle changes in curvature in product shapes. Consequently, recent research has explored the integration of curvature and entropy to quantify the complexity of three-dimensional shapes [30–36].

However, Eibl-Eibesfeld [22] contends that order is the property of reducing the information of a cognitive object. Lugo et al. [37] quantified order by defining it as factors that reduce the information of the perceived shape, using Gestalt principles such as ‘proximity’ and ‘continuity’ in two-dimensional shapes, calculated by the distance or the angle formed by tangents at any two points on the shape. Furthermore, considering that ‘symmetry’ is one of the Gestalt principles and a major factor in order [25] and has a significant impact on aesthetic preferences compared to other information reduction factors [37], Kato et al. [23] quantified order by defining symmetry as the information reduction factor of the perceived shape and quantified it using mirror and rotational symmetries in two-dimensional shapes. Previous research has quantified order in two-dimensional shapes by quantifying information reduction factors related to shape, including symmetry. However, unlike studies on complexity, there has been a lack of research on quantifying order in three-dimensional shapes. Attempts have been made to quantify symmetry as a major factor in order [25] in three-dimensional shapes. Among human symmetry perceptions, ‘mirror symmetry’ is more prominent and is considered more important than other symmetries such as rotational and translational symmetries [25,38–42]. Therefore, conventional studies have focused on the quantification of mirror symmetry. The following is a summary of studies on the quantification of mirror symmetry in three-dimensional geometry.

Several studies have attempted to quantify it. Existing studies have quantified symmetry by calculating the difference in the number of voxels [43–48] when dividing three-dimensional voxel shapes by arbitrary planes into two parts. However, as mentioned earlier, Farin et al. [29] have emphasized the importance of curvature in design. In the field of design, polygon shapes are frequently used as they provide more degrees of freedom to represent diverse and smooth surfaces [49,50]. Therefore, it was challenging to apply these methods to the design evaluation in this study. Conversely, in existing studies on three-dimensional polygonal shapes, a plane at the center of gravity of the target shape is defined and the mirror symmetry of the shape is quantified by comparing the difference in distance from the plane at two points where the target shape intersects a perpendicular line of the plane [37,51,52]. However, these methods cannot be used for shapes that lack two intersection points with the symmetry plane, such as those with holes or only one side.

Considering this, the goal of this study is to introduce a quantifiable ‘order’ index applicable to all three-dimensional polygonal shapes. This index quantifies ‘symmetry’ using curvature, which is an important factor in design [28]. Previous studies [25,38–42] have shown that mirror symmetry is more prominent and significant than other types of symmetry (rotational and translational) in human symmetry perception. Therefore, this study focuses on quantifying mirror symmetry to derive an index for quantifying the order. This index will contribute to the development of generative design by enabling the evaluation of previously non-assessable shapes.

The remainder of this paper is organized as follows: Section 2 outlines the method for calculating order in three-dimensional shapes using curvature and mirror symmetry. Section 3 illustrates the sensory evaluation experiment conducted to validate the effectiveness of the calculated index of order. Section 4 presents the conclusions drawn from this study.

2. 'Order' Quantification Index for Three-Dimensional Shapes

2.1. Proposal for an Index for Quantifying 'Order' in Three-Dimensional Shapes Using Curvature

In this study, the proposed index was computed using the Casorati curvature [53]. The rationale for this selection is rooted in the research conducted by Matsuyama et al. [33], which revealed that the entropy of Casorati curvature exhibited a high and stable coefficient of determination with sensory evaluations of 'complexity' in three-dimensional shapes, compared to other curvatures, across variations in shape and discretization parameters. The Casorati curvature C_c is calculated using the maximum principal curvature k_1 and the minimum principal curvature k_2 as follows:

$$C_c = \frac{\sqrt{k_1^2 + k_2^2}}{2} \quad (1)$$

Appendix A provides a detailed calculation of the Casorati curvature in three-dimensional shapes (polygon models).

2.2. Method for Calculating the Discrete Probability Distribution of Curvature

In this study, the discrete-type probability distribution of the curvature was calculated by distributing the continuous curvature into multiple bins using a discretization process. The proposed index was computed using this distribution. In this study, to determine the essential discretization parameters, namely, the maximum and minimum area values and the number of bins, the conventional curvature discretization methods were used as follows [30,31,33]:

1. Curvature at all vertices for all shapes under evaluation were calculated.
2. The percentile intervals [0.003%, 99.997%] of the curvatures were calculated. This interval was determined with reference to the mean ± 4 (standard deviations) for a normal distribution. This aims to ignore the curvatures as outliers resulting from the subdivision of three-dimensional shapes into polygons, as mentioned in Section 3.1.1.
3. Curvatures within the specified percentile intervals [0.003%, 99.997%] were divided into a number of bins (positive integers). Curvatures above the maximum and below the minimum of the same interval were assigned to bins with the largest and smallest curvatures, respectively.
4. Integers from 2 to 20 were used as candidates for the number of states.

2.3. Method for Calculating the Quantification Index of 'Order'

This study quantifies mirror symmetry in shapes using curvature and computes a quantification index of 'order' in three-dimensional shapes. A method for computing the proposed index is given below:

1. Casorati curvature on the surfaces of the three-dimensional shape was calculated.
2. The centroid G of the three-dimensional shape was set to coincide with the origin of the xyz -space.
3. The shape was divided into two parts with respect to an arbitrary plane F (Figure 1).
4. The curvature distributions (discrete probability distributions) P and Q for the two surfaces obtained after the division (Figure 2a,b) were calculated.
5. The Jensen–Shannon distance (hereinafter referred to as the JS distance) representing the dissimilarity of curvature distributions for the two surfaces obtained with respect to the arbitrary plane F was calculated. This value was multiplied by -1 to obtain the quantification index of 'order' in the shape, denoted as S_F .

$$S_F = -\sqrt{D_{JS}(P \parallel Q)} = -\sqrt{\frac{D_{KL}\left(P \parallel \frac{P+Q}{2}\right) + D_{KL}\left(Q \parallel \frac{P+Q}{2}\right)}{2}} \quad (2)$$

where $D_{JS}(P \parallel Q)$ represents the JS divergence of P and Q , while $D_{KL}(P \parallel Q)$ represents the KL divergence of P and Q . Specifically, $D_{KL}(P \parallel Q) = \sum_i P(i) \log \frac{Q(i)}{P(i)}$, where $P(i)$ and $Q(i)$ represent the probability at event i in probability distributions P and Q , respectively. S_F increases when the similarity between the two curvature distributions is high (i.e., when the JS distance is small). In this context, the proposed index S can also be calculated as the average of ‘mirror symmetry’ for multiple arbitrary planes F_1, F_2 , and F_3 , providing a measure of ‘order’ that considers multiple surfaces.

$$S_{F_1, F_2, F_3} = \overline{S_{F_1} + S_{F_2} + S_{F_3}} \tag{3}$$

Note that the index of ‘order’ that accounts for multiple surfaces arises from the human characteristic of evaluating the mirror symmetry of shapes from multiple angles [38–40,54].

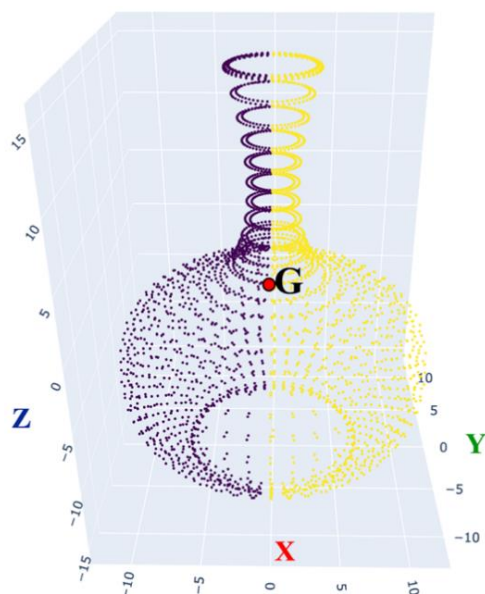


Figure 1. Division of a three-dimensional shape into two parts by yz -plane (G is the centroid of the shape and different colors represent divided surfaces).

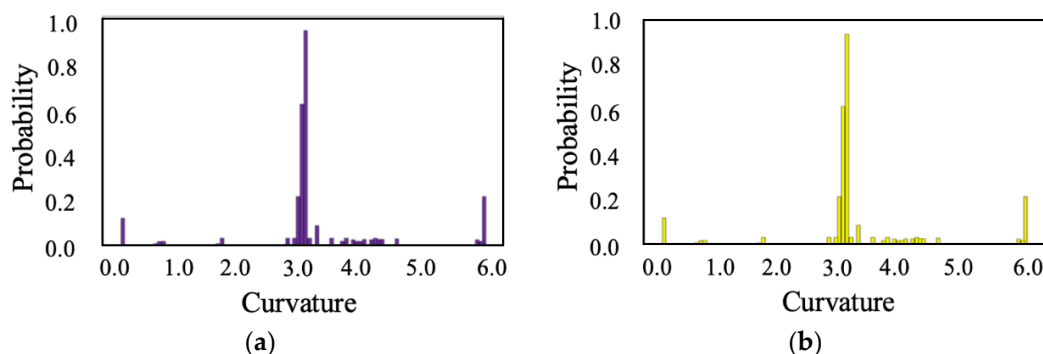


Figure 2. Curvature (a) Distribution P and (b) Distribution Q .

3. Sensory Evaluation Experiment

3.1. Experimental Method

3.1.1. Sample Shapes

In this experiment, we evaluated the following shapes: (1) extruded, (2) rotated, and (3) vase shapes. The methods for creating the sample shapes and the reasons for selecting each shape are described below. We divided the entire shape into polygons of equal area to calculate the curvature (hereafter referred to as polygon equal division) for all three sample

shapes. The two main reasons for performing polygon equal division are as follows: First, the calculation of the Casorati curvature involves the polygon area; if the shape's polygon area is uneven, it may affect the curvature values. The second reason pertains to the quantification index of order in this study, which focuses on the distribution of curvature at the shape's vertices and evaluates 'mirror symmetry'. It is essential for the vertices to be evenly distributed without bias in the upper, lower, left, and right parts of the shape to prevent any influence on the evaluation of 'mirror symmetry'. Therefore, in this study, we used the advancing-front method [55] to perform equal polygon division on the sample shapes. Although other popular methods for polygon equal division such as Delaunay triangulation [55] exist, the advancing-front method offers the advantage of accurately generating polygons even at the edges of the shape, making it suitable for this experiment, which uses shapes with edges [55,56]. In other methods, polygons generated from the centers of faces can result in irregular shapes and sizes at the edges, leading to inaccurate polygon division [55]. Therefore, this study conducted sensory evaluation experiments using shapes that underwent the advancing-front method for equal polygon division. In this study, we conducted sensory evaluation experiments using the same method on equally divided polygonal shapes. However, we excluded the meshing of shapes with minute irregularities because the meshes were damaged in areas with significant curvature variations. This is because the radius of curvature was too small compared to the size of the mesh set during meshing. Although it is possible to address this by making the mesh finer, this correspondence would lead to the evaluation of fine irregularities that humans cannot recognize, resulting in a loss of correlation between sensory evaluation and the index. In this study, we prioritized maintaining the mesh size equal to that used in previous studies [33,57] that evaluated human perception of three-dimensional polygonal shapes.

1. Extruded shape

The extruded shape is a three-dimensional surface shape created from a two-dimensional closed curve using a fundamental three-dimensional CAD shape-creation method known as extrusion. In this experiment, we used 50 curved shapes based on Birkhof's shapes [20,31–33], originally created by Ujii [57]. Subsequently, we generated three-dimensional sample shapes by extruding these curves in a direction perpendicular to the original shape using Autodesk Fusion 360. The extrusion length for each shape was established by referencing previous studies that conducted sensory evaluations with similar shapes [31–33,57]. The length is set to twice the maximum diameter of each curved shape. In this experiment, we used 49 shapes as samples (excluding shapes damaged during the polygon equal division process), as shown in Figure 3.

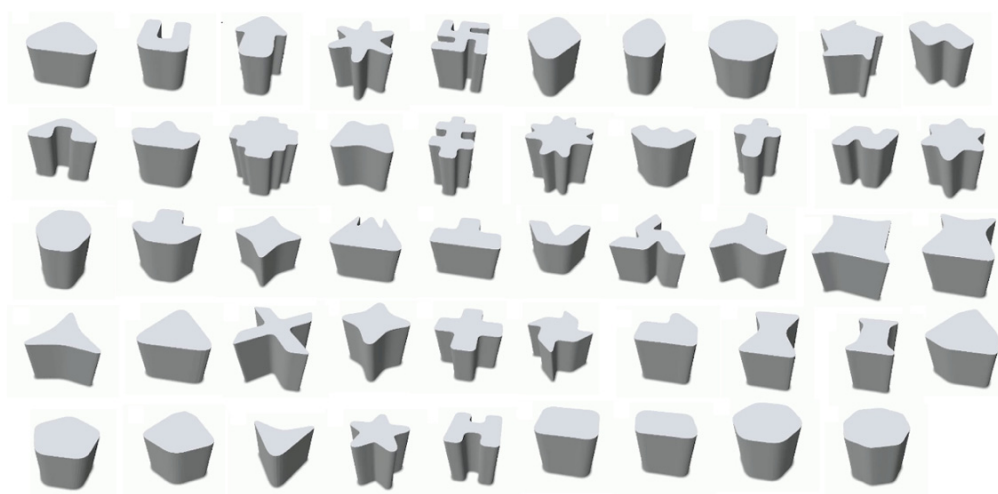


Figure 3. Extruded shape.

2. Rotated shape

Rotated shapes are three-dimensional surface shapes generated from two-dimensional closed curves using the fundamental three-dimensional CAD shape creation method, known as rotation. In this experiment, we used the same set of 50 two-dimensional closed curve shapes that were used for the extruded shapes. These shapes were created by rotating the right side of each two-dimensional shape 360° around a vertical axis passing through the centroid of the two-dimensional shape using Autodesk Fusion 360. In this experiment, we used 46 shapes as samples (excluding shapes damaged during the polygon equal division process), as shown in Figure 4.

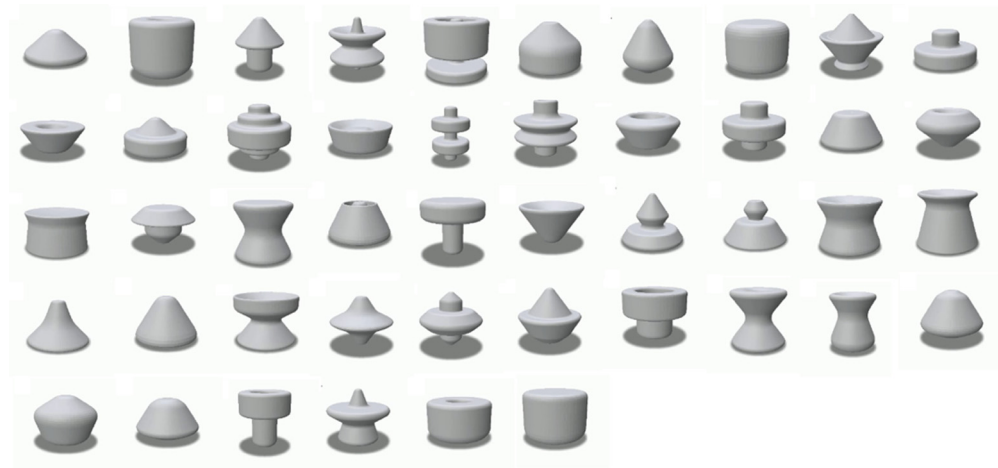


Figure 4. Rotated shape.

3. Vase shape

The vase shape is a product characterized by a high degree of shape freedom, often featuring distinctive attributes such as ‘holes’ and ‘twists’. In this experiment, we used 50 three-dimensional vase shape datasets: 25 provided by free three-dimensional models [58] and 25 provided by CGTrader [59]. To exclude the inner surfaces of the vases that were not visually perceptible, the vase openings were sealed with flat surfaces. However, to ensure that the participants could recognize the openings when they looked at the presented vase shape, only the edges of the openings were sealed. Shapes with fine surface texture were excluded because evaluating surface texture added unnecessary complexity to the evaluations of the silhouettes of the three-dimensional shapes, which were the focus of this study. Based on the above, we used 33 shapes as samples (excluding shapes damaged during the polygon equal division process), as shown in Figure 5.

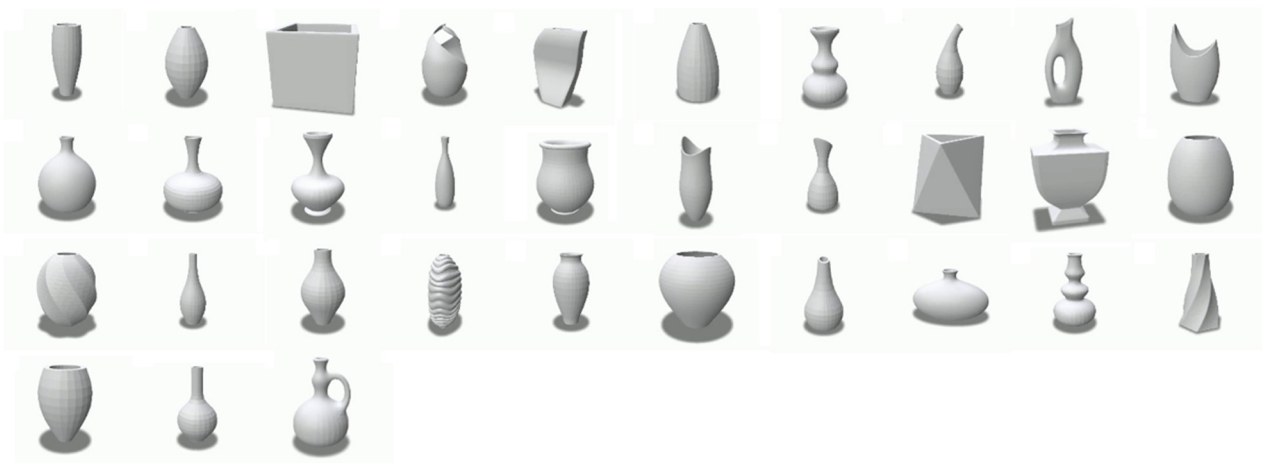


Figure 5. Vase shape.

All the extruded shapes exhibited mirror symmetry for planes perpendicular to the extrusion direction (which was set as the vertical axis in this experiment). However, for planes parallel to the extrusion direction, some shapes exhibited mirror symmetry, whereas others did not. All rotated shapes exhibited mirror symmetry concerning planes parallel to the rotation axis (which was oriented vertically in this experiment). However, for planes perpendicular to the rotation axis, some shapes exhibited mirror symmetry, whereas others did not. Regarding vase shapes, irrespective of whether they included planes containing the horizontal axis (set, as the bottom of the vase is parallel to it) or planes containing the vertical axis, some shapes exhibited mirror symmetry, whereas others did not. In this experiment, we selected three types of sample shapes, each with different orientations and numbers of symmetrical planes to assess the effectiveness of the proposed index.

3.1.2. Experimental Conditions

This experiment was conducted under the following conditions:

1. Presentation Method: Gray-colored sample shapes were displayed on a white background in an online survey. To assess the participants' response accuracy, 10 shapes were randomly selected from the sample shapes and presented without duplication. Each shape was rotated at a consistent speed (vertical axis: 9.0 s per rotation).
2. Sensory Evaluation Method: For assessing 'order', a 5-point Likert scale was used, which included the following options: 'No order: 1', 'Slightly no order: 2', 'Undecided: 3', 'Slightly order: 4', and 'Order: 5'. This scale was chosen for its ease of use for ordinary people [60] and its frequent use in previous studies [14,20,23,36,37,61], which investigated shape-related features such as order and symmetry.
3. Participants: 110 participants (70 males and 40 females) participated in the experiment. Participants whose absolute differences in sensory evaluation scores for the 10 randomly selected shapes exceeded a cumulative total of 10 were excluded from the analysis, as were those who were assigned identical ratings for all shapes. Consequently, data from 85 participants were considered for the 'extruded shapes', data from 70 participants for the 'rotated shapes', and data from 71 participants for the 'vase shapes'.

3.2. Experimental Results and Discussion

3.2.1. Extruded Shape

First, we present the results and discuss the variations in the coefficient of determination concerning the number of segmented surfaces. Figure 6 illustrates the relationship between the proposed index and the sensory evaluations of the order for different numbers of bins (integers from 2 to 20) for the extruded shapes. In this study, the center of gravity of the shape was set at the origin of the xyz -space, and the shape was oriented such that the extrusion direction was aligned with the z -axis. We computed seven proposed indices, S_{xy} , S_{yz} , S_{zx} , $S_{xy,yz}$, $S_{yz,zx}$, $S_{zx,xy}$, and $S_{xy,yz,zx}$, where the subscripts xy , yz , and zx mean xy -plane, yz -plane, and zx -plane, respectively. From Figure 6, it can be observed that the maximum coefficient of determination with the sensory evaluation values of order is achieved when the number of bins is 20, and the proposed index $S_{yz,zx}$ is computed, resulting in a coefficient of determination of 0.36. Furthermore, Figure 6 shows that considering the proposed indices related to symmetry in the xy -plane ($S_{xy,yz}$, $S_{zx,xy}$, and $S_{xy,yz,zx}$) and not considering them (S_{yz} , S_{zx} , and $S_{yz,zx}$) produces similar results. The extruded shapes exhibited complete mirror symmetry with respect to planes orthogonal to the extrusion direction (xy -plane). Therefore, the S_{xy} values were nearly zero for all shapes and had little impact on the index. Furthermore, Figure 6 shows that the coefficient of determination with the sensory evaluation values of order is greater compared to the proposed index $S_{yz,zx}$ considering mirror symmetry about the yz -plane and zx -planes compared to the proposed index S_{yz} or S_{zx} considering mirror symmetry about the yz -plane or zx -planes. This could be because humans evaluate the mirror symmetry of shapes from multiple angles and not just from a single perspective [38–40,54]. Therefore, considering mirror symmetry

from multiple facets during segmentation likely contributed to the increased coefficient of determination between the proposed indices and the sensory evaluation values of the order.

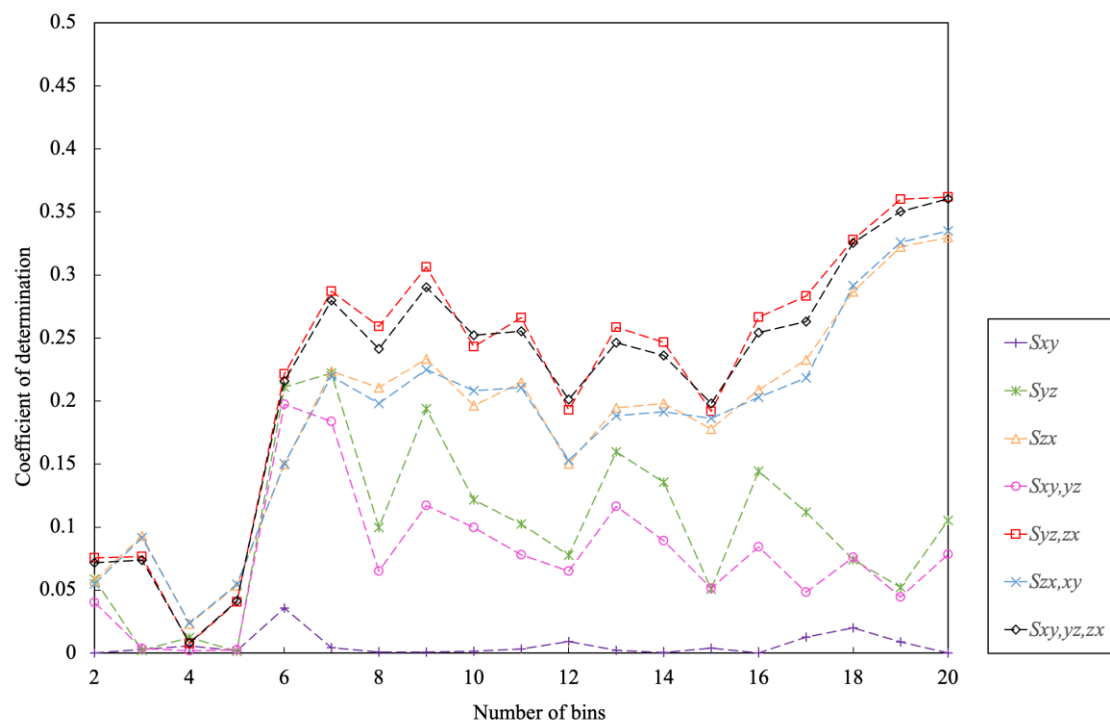


Figure 6. Relationship between the number of bins and coefficient of determination in extruded shapes.

Next, we examined the proposed index $S_{yz,zx}$, which exhibited the highest coefficient of determination among the seven proposed indices. We examined the reasons for the coefficient of determination's variations with bin count, particularly for different bin counts. Figure 6 indicates that the coefficient of determination for $S_{yz,zx}$ is the smallest when the number of bins is four. Figure 7 shows a scatter plot of the proposed index and sensory evaluation values of the order for this case. The red-colored plots (Shapes A, B, and C) are discussed below. This figure shows that the proposed index takes values close to zero for almost all the shapes, indicating that the index values vary little between the shapes. To investigate further, we consider multiple shapes (A, B, and C) as examples and provide contour plots of their curvature as well as histograms of the curvature of each segment when the shape is divided into two, as shown in Figures 8–10. These figures include contour plots of curvature from four viewpoints (top-down perspective and perspectives along the x -axis, y -axis, and z -axis) and histograms of curvature for each part when segmented along the yz -plane and zx -plane. These figures show that in bin 4, all curvatures of the side portions, except the curvature of the edges, are assigned to the same bins, and there is almost no difference in the curvature distribution in each part of the divided geometry. Consequently, the values of the proposed index increased (became closer to 0) for almost all shapes, and the differences in index values between shapes diminished, leading to a smaller coefficient of determination between the proposed index and the sensory evaluation values of order. Furthermore, we examined the contour plots and histograms of curvature for bins 2, 3, and 5, which showed similar behavior to that observed for bin 4. When the number of bins is small, the curvatures assigned to them become biased, causing the correlation coefficient of determination to become unstable and fluctuate significantly. In contrast, for bin numbers 6 and above, the coefficient of determination remained consistently high, suggesting that six or more bins were necessary in this experiment. Even with six or more bins, there is still a slight variation in the correlation coefficient of determination between even and odd numbers of bins. This may be because when the number of bins is even, the

values around the most common curvature of 0 are divided into two bins, leading to an overestimation of the index and a decrease in the correlation coefficient of determination.

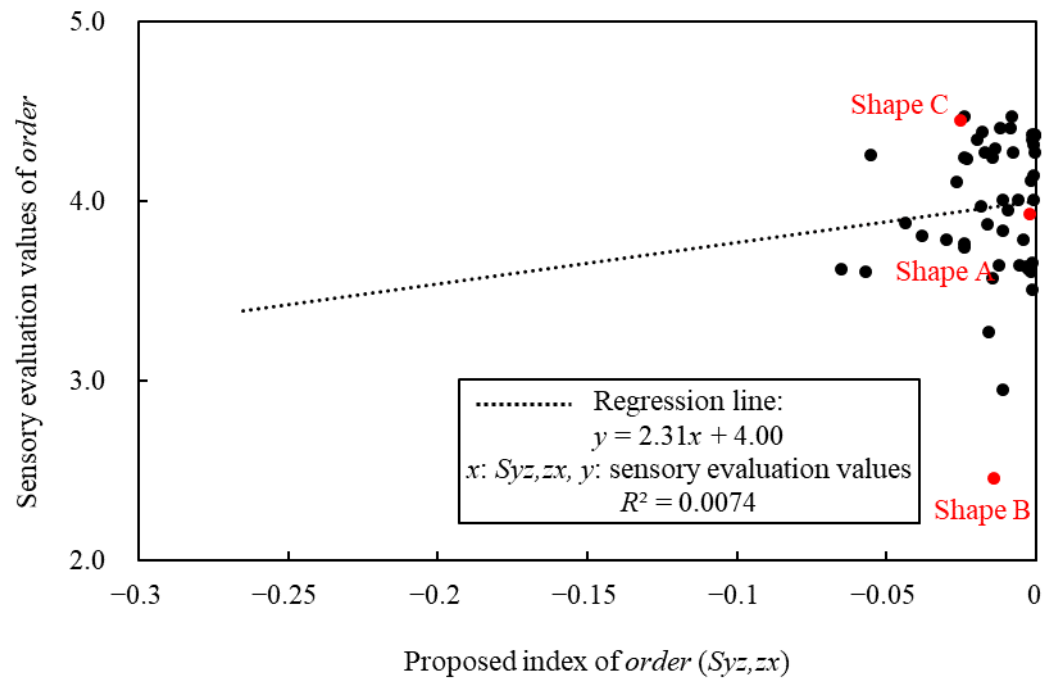


Figure 7. Relationship between the proposed index $S_{yz,zx}$ and sensory evaluation values of ‘order’ in bin number 4.

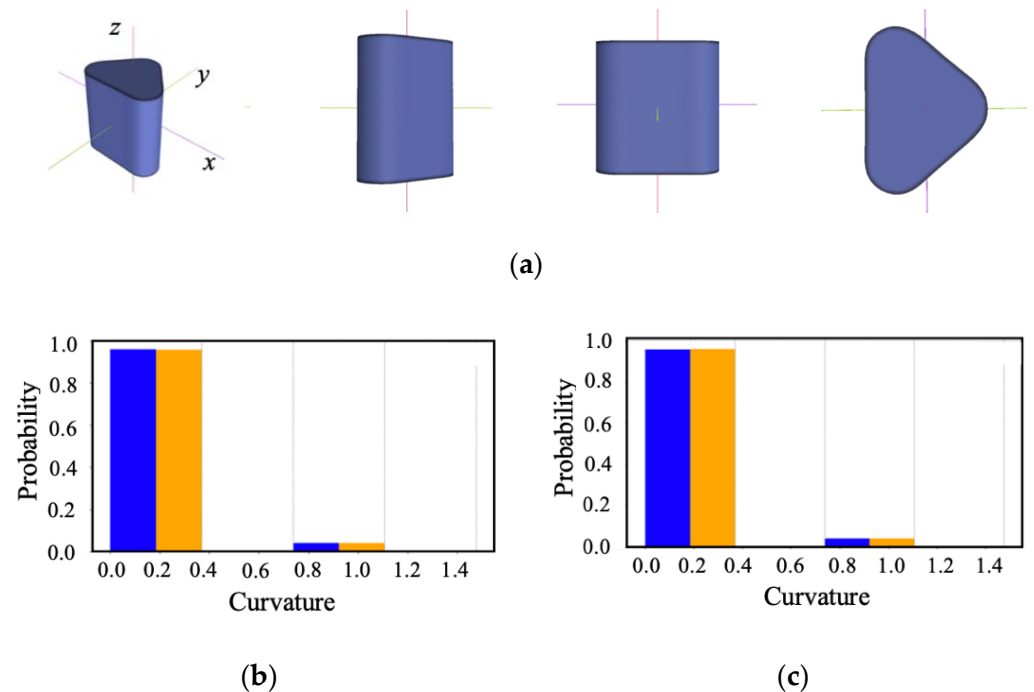


Figure 8. Contour plots and curvature distributions in Shape A: (a) contour plots from different perspectives; (b) curvature distribution of each part (blue and orange) obtained for the yz -plane; (c) curvature distribution of each part (blue and orange) obtained for the zx -plane.

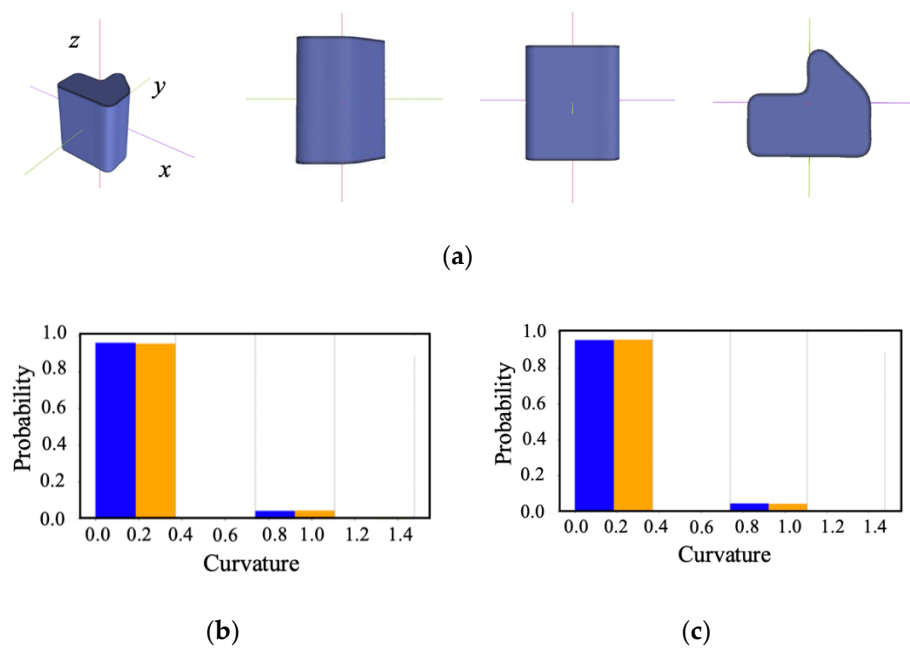


Figure 9. Contour plots and curvature distributions in Shape B: (a) contour plots from different perspectives; (b) curvature distribution of each part (blue and orange) obtained for the yz -plane; (c) curvature distribution of each part (blue and orange) obtained for the zx -plane.

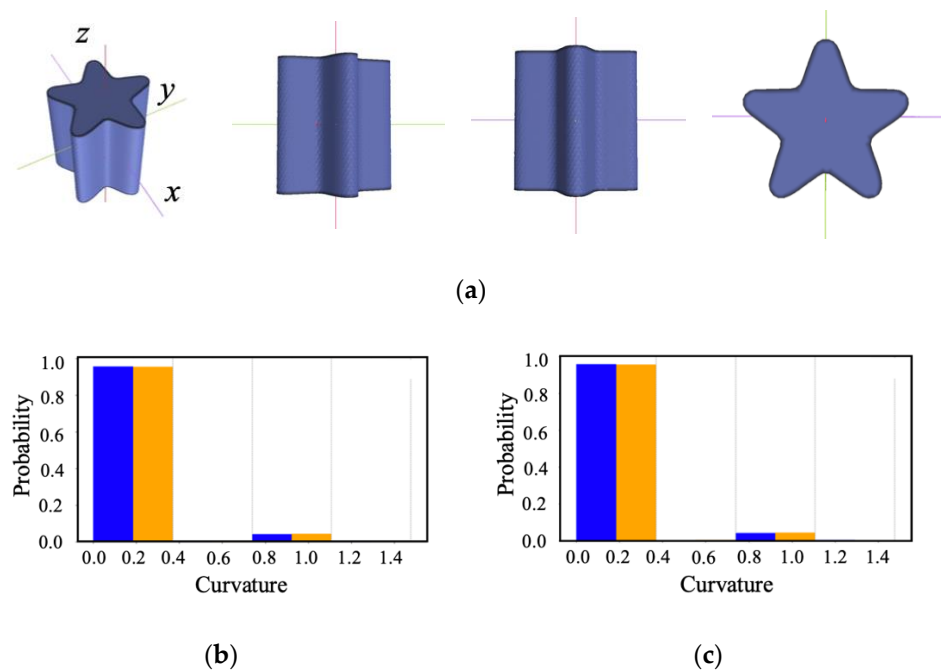
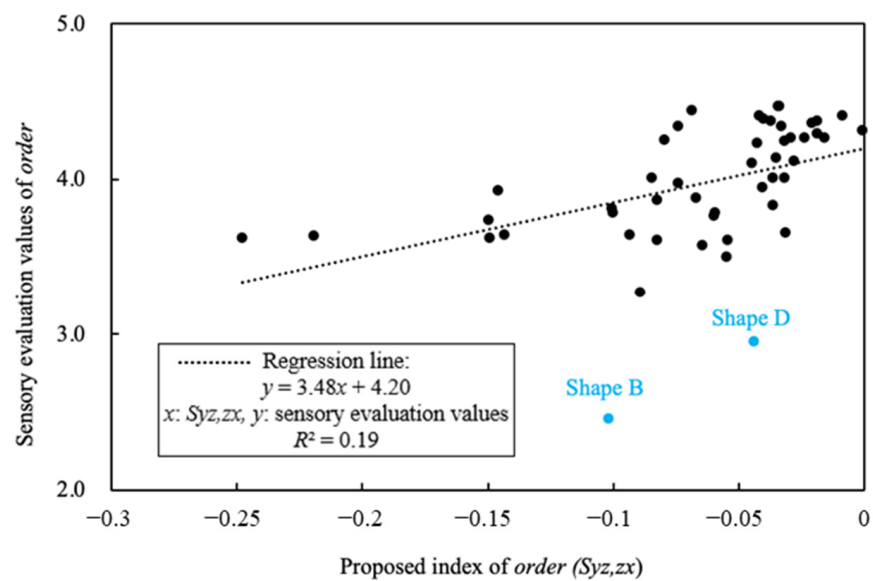


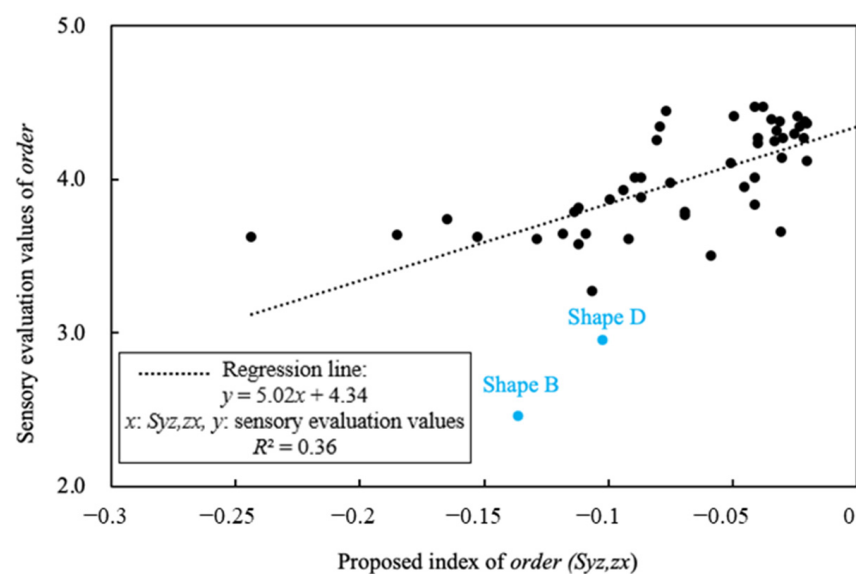
Figure 10. Contour plots and curvature distributions in Shape C: (a) contour plots from different perspectives; (b) curvature distribution of each part (blue and orange) obtained for the yz -plane; (c) curvature distribution of each part (blue and orange) obtained for the zx -plane.

Figure 11a,b shows the scatter plots of the proposed index and sensory evaluation values for the cases with the lowest coefficient of determination at bin number 15 and the highest coefficient of determination at bin number 20. The blue-colored plots (Shapes B and D) are discussed below. The two scatter plots show that as the bin number changed from 15 to 20, the values of the proposed index for Shapes B and D became smaller than those of the other shapes, approaching the regression line. This suggests that the coefficient of determination increases significantly at bin number 20. The contour plots of

the curvature and histograms of the curvature distributions for Shapes B and D are shown in Figures 12–15. Figures 12 and 14 show contour plots and histograms in bin 15 for Shapes B and D, respectively. In addition, Figures 13 and 15 show contour plots and histograms at bin 20 for Shapes B and D, respectively. These figures reveal that at bin 20, the large curvature values (red regions in the contour plots) found in the side cavities, which were indistinguishable at bin 15, could now be distinguished from the other side curvatures. This is confirmed by the fact that in the histograms of Figures 12 and 13, when the number of bins changes from 15 to 20, a new distribution appears in the fourth bin from the left, and in the histograms of Figures 14 and 15, when the number of bins changes from 15 to 20, a new distribution appears in the third bin from the left. Consequently, the differences in the curvature distributions for each part of the shapes divided on the zx -plane become significant in bin 20, causing the proposed index values to become smaller than those at bin 15 (i.e., the proposed index values become closer to the sensory evaluation values); therefore, the coefficient of determination increases at bin 20.

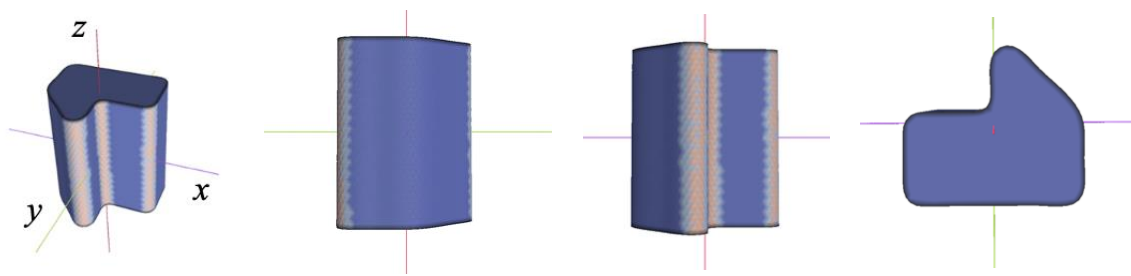


(a)

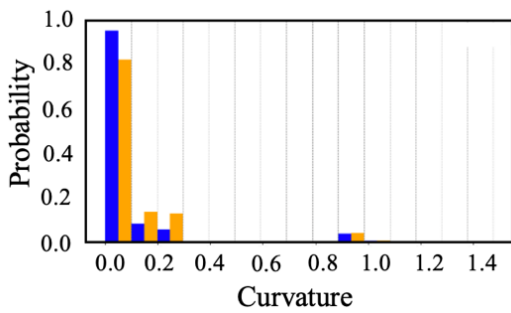


(b)

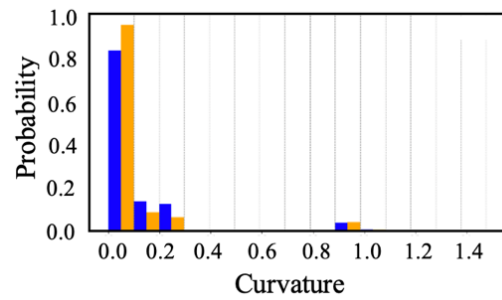
Figure 11. Relationship between the proposed index $S_{yz,zx}$ and sensory evaluation values of 'order' in (a) bin number 15 and (b) bin number 20.



(a)

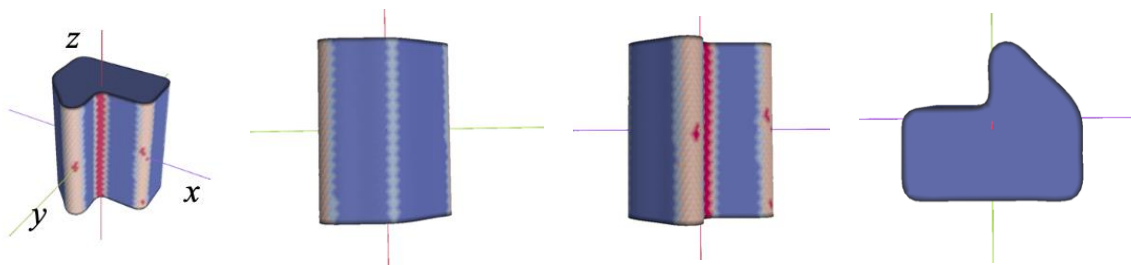


(b)

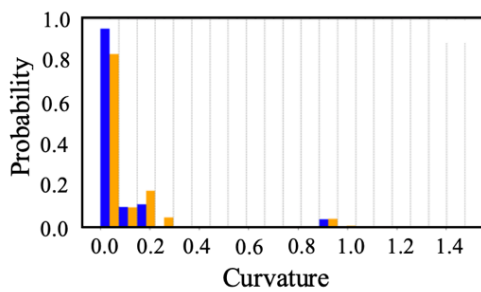


(c)

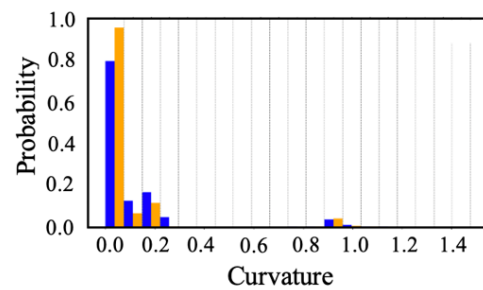
Figure 12. Contour plots and curvature distributions in Shape B in bin number 15: (a) contour plots from different perspectives; (b) curvature distribution of each part (blue and orange) obtained for the yz -plane; (c) curvature distribution of each part (blue and orange) obtained for the zx -plane.



(a)



(b)



(c)

Figure 13. Contour plots and curvature distributions in Shape B in bin number 20: (a) contour plots from different perspectives; (b) curvature distribution of each part (blue and orange) obtained for the yz -plane; (c) curvature distribution of each part (blue and orange) obtained for the zx -plane.

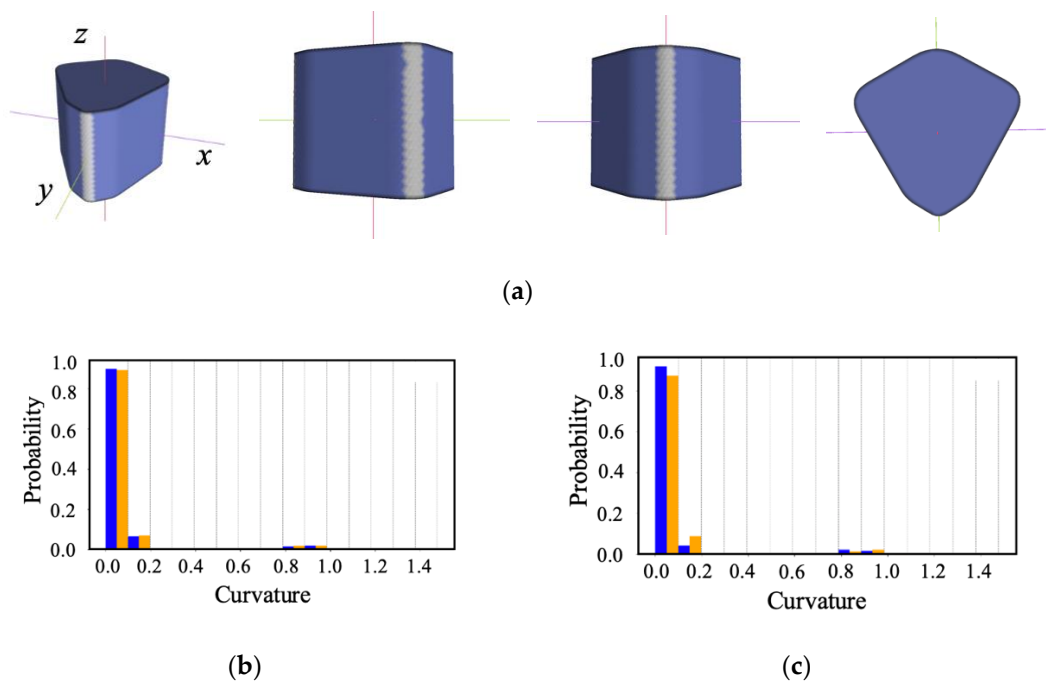


Figure 14. Contour plots and curvature distributions in Shape D in bin number 15: (a) contour plots from different perspectives; (b) curvature distribution of each part (blue and orange) obtained for the yz -plane; (c) curvature distribution of each part (blue and orange) obtained for the zx -plane.

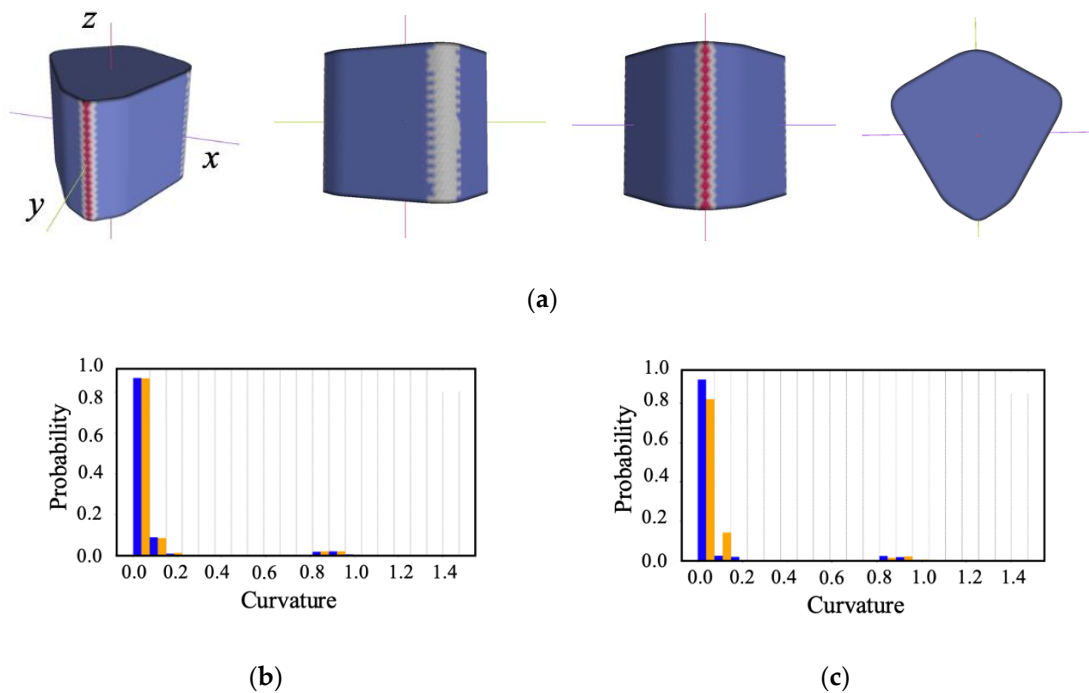


Figure 15. Contour plots and curvature distributions in Shape D in bin number 20: (a) contour plots from different perspectives; (b) curvature distribution of each part (blue and orange) obtained for the yz -plane; (c) curvature distribution of each part (blue and orange) obtained for the zx -plane.

Finally, we discuss the proposed index $S_{yz,zx}$ (bin number 20), which exhibited the highest coefficient of determination with the order sensory evaluation value. Figure 16 shows a scatter plot of $S_{yz,zx}$ (bin number 20) and the order of the sensory evaluation value. The yellow-colored plots (Shapes B, C, D, E, F, G, and H) are discussed below. Figure 16 shows that the coefficient of determination was 0.36, indicating a moderate level

of correlation between $S_{yz,zx}$ (bin number 20) and the order of sensory evaluation values in the case of extruded shapes. Now, we examine shapes for which the proposed index and sensory evaluation values differ significantly.

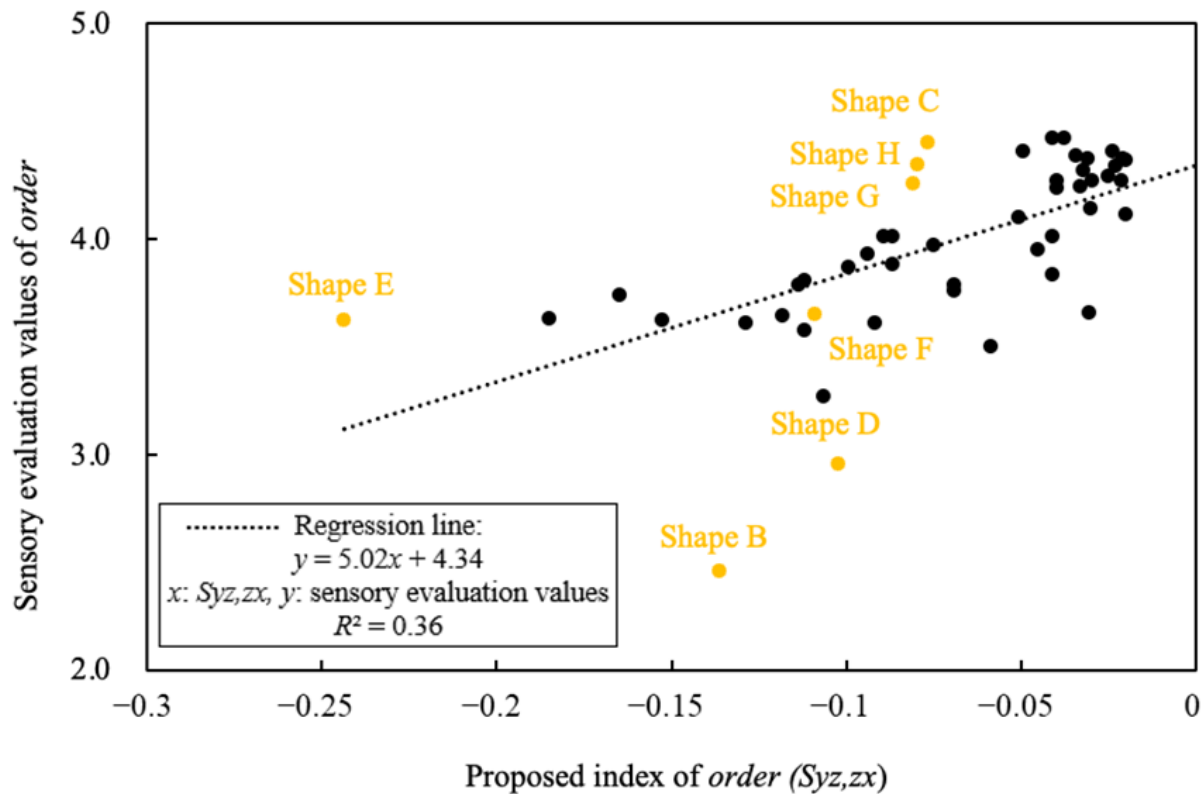


Figure 16. Relationship between the proposed index $S_{yz,zx}$ and sensory evaluation values of ‘order’ in bin number 20.

■ Shapes for which the proposed index overestimates order

In Figure 16, it is evident that the proposed index tends to overestimate the order for shapes resembling Shapes B and D. Figure 17 displays the histogram of the shape’s curvature of each part for Shape B as well as the contour plots of the shape’s curvature. Similarly, for Shapes E and D, the contour plots of the shape’s curvature and the histogram of the shape’s curvature are shown in Figures 18 and 19. The shape is viewed from multiple angles, as shown in Figure 20.

First, we consider Shape B. Figure 17 shows that Shape B is the only sample shape that lacks mirror symmetry in the plane parallel to the extrusion direction. Figure 16 shows that it received the lowest-order sensory evaluation values. However, as observed from the contour maps and histograms in Figure 17, irrespective of whether the shape is divided along the zx -plane or yz -plane, there is little difference in the curvature distribution. Therefore, the value of the proposed index is probably close to the average (rather than the minimum). For comparison, Figure 18 displays the contour maps and histograms of the curvature for Shape E, where the index value is at its lowest. It is evident from Figures 17 and 18 that there is no discernible difference between the curvature distribution of each part in Shape B when we compare the histogram of Shape E with that of Shape B, where the difference in curvature distribution is noticeably larger and the index value is the smallest when divided in the yz -plane. Furthermore, Figure 17 shows that although Shape B does not have mirror symmetry with respect to the plane parallel to the extrusion direction, it does not have sharp convex areas, and almost all the existing convex areas have moderately large curvatures (pink areas in the contour plots) that are distributed in the same area. Therefore, when the shape is divided into the yz - and zx -planes, the large curvature (the red portion in the contour plots) that is present in the concave portion on

the side appears only on one side, but the magnitude of the curvature in the other portions is not significantly different. This led us to believe that the shape did not exhibit a large difference in curvature distribution. Therefore, the proposed index overestimates the order.

Shape D, shown in Figure 19, has sharp convexity in only one part of the shape, and it has the second-lowest sensory evaluation value of order, as shown in Figure 16. However, as can be seen from the contour plots and histograms in Figure 19, there is no significant difference in the distribution of the curvature in each of the divided sections, suggesting that the value of the proposed index is close to the average (rather than close to the minimum). Figure 21 shows how the shape is viewed from multiple angles for Shape F, which has the same level of value for the proposed index as Shape D and is on the regression line as a comparison object to illustrate why the sensory evaluation value of the order for Shape D is low. In Figures 20 and 21, the two shapes are similar in that only one part of the shape has a sharp convexity. However, when Shape D was presented to the subject in the experiment, it was challenging for the subject to recognize the mirror symmetry of the shape when the shape was viewed from the angle shown in Figure 22. The subject judged the shape to have no mirror symmetry about the plane parallel to the extrusion direction and evaluated the order instead. The reason why Shape F does not exhibit this phenomenon is that Shapes D and F have similar shapes, but Shape F has a sharper and more pointed shape. When the shape is presented in the experiment, the subject may judge it to have a shape that does not have mirror symmetry with respect to a plane parallel to the extrusion direction. This may have facilitated the recognition of the mirror symmetry with respect to the plane parallel to the extrusion direction when the shapes were presented in the experiment (Figure 21). Therefore, we believe that the subjects underestimated the order of Shape D and overestimated the order of the proposed index.

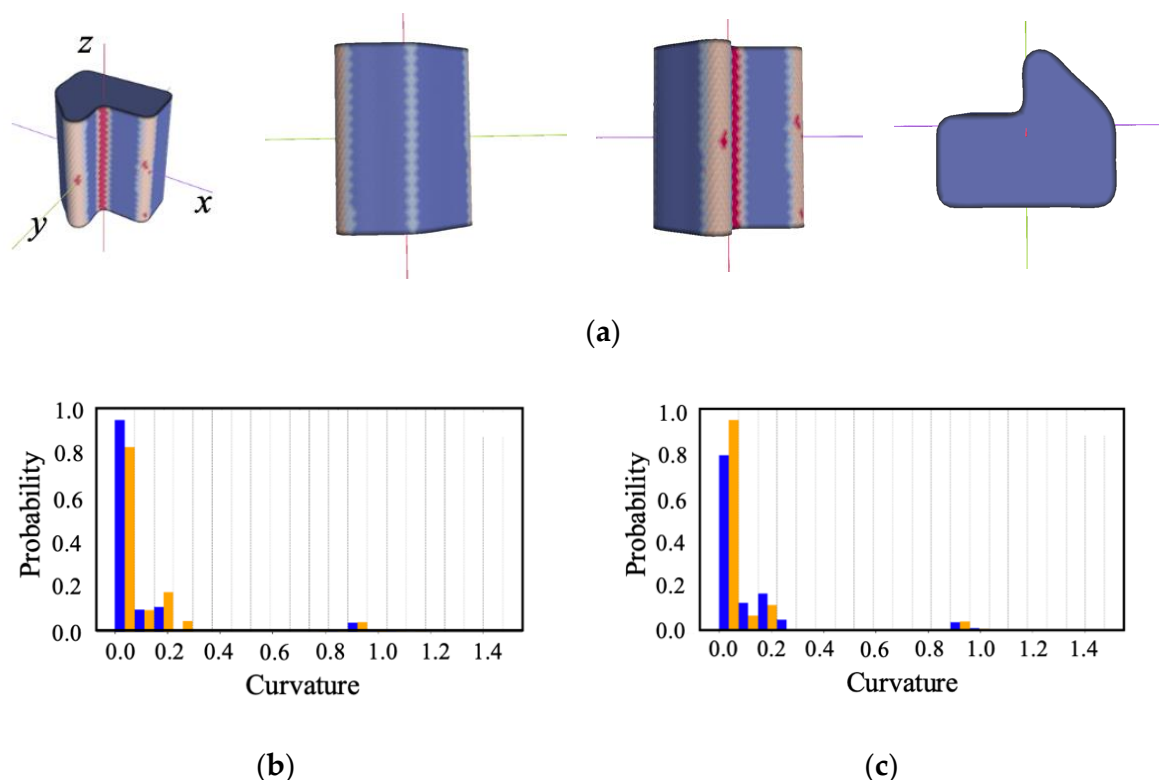


Figure 17. Contour plots and curvature distributions in Shape B: (a) contour plots from different perspectives; (b) curvature distribution of each part (blue and orange) obtained for the yz -plane; (c) curvature distribution of each part (blue and orange) obtained for the zx -plane.

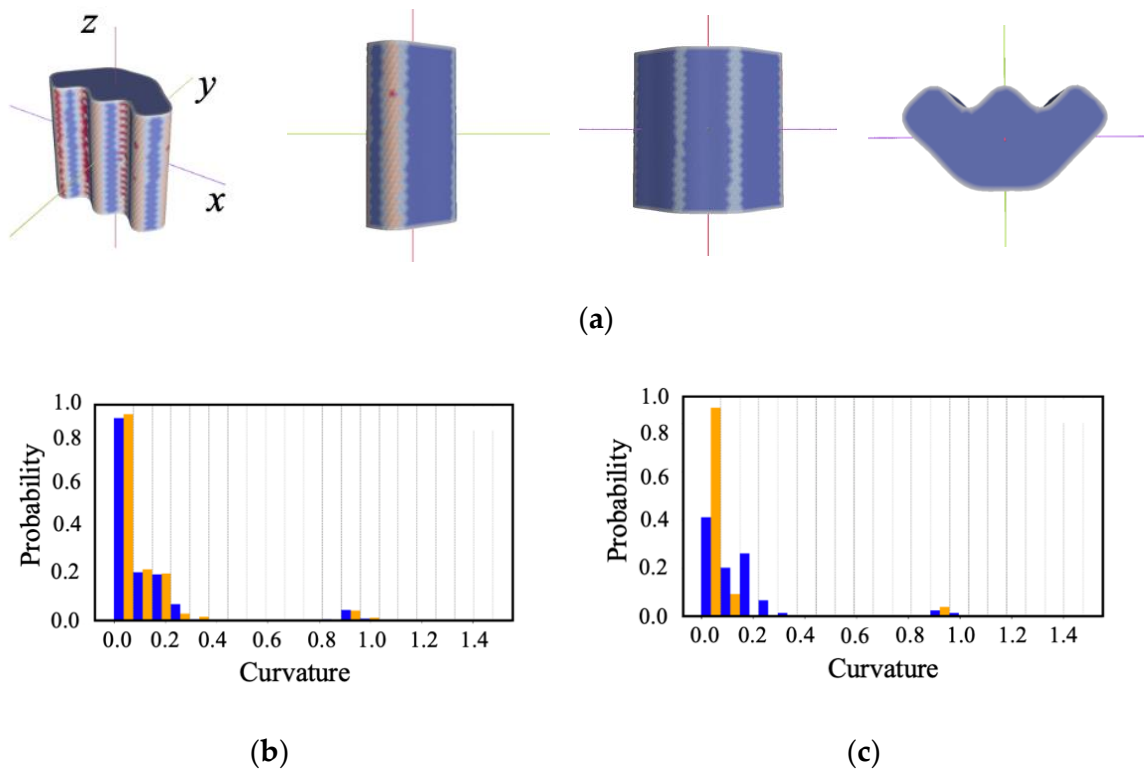


Figure 18. Contour plots and curvature distributions in Shape E: (a) contour plots from different perspectives; (b) curvature distribution of each part (blue and orange) obtained for the yz -plane; (c) curvature distribution of each part (blue and orange) obtained for the zx -plane.

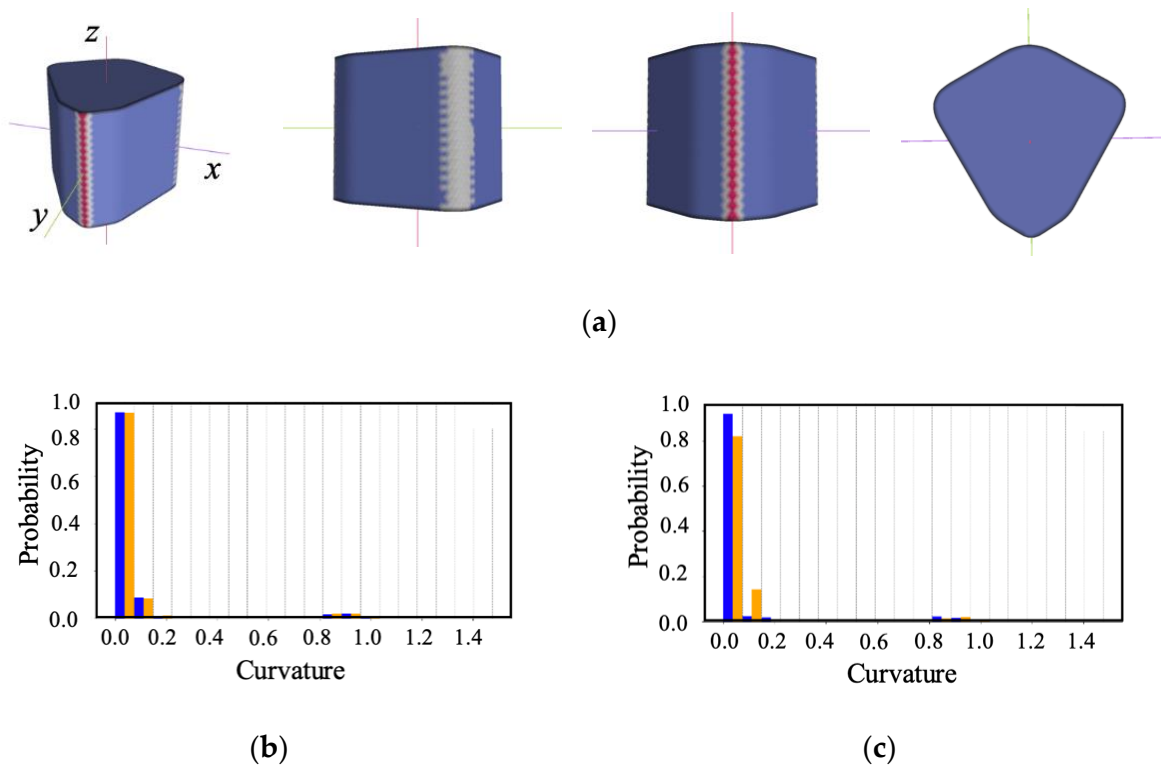


Figure 19. Contour plots and curvature distributions in Shape D: (a) contour plots from different perspectives; (b) curvature distribution of each part (blue and orange) obtained for the yz -plane; (c) curvature distribution of each part (blue and orange) obtained for the zx -plane.

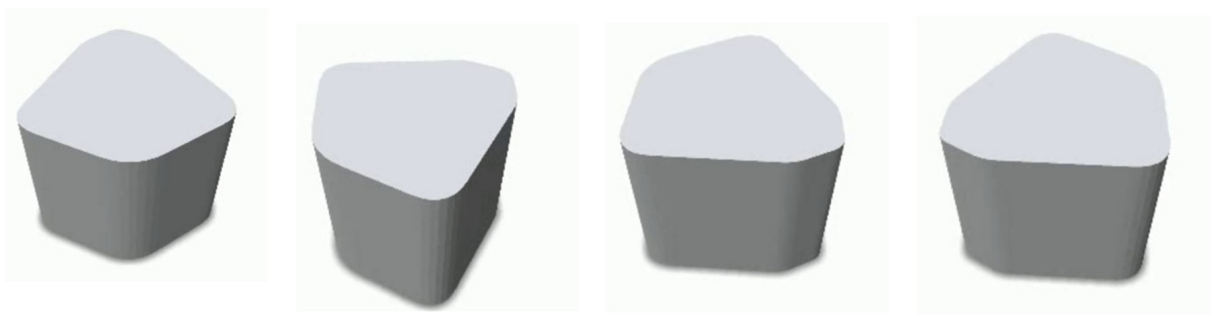


Figure 20. Appearance of Shape D when viewed from multiple perspectives.

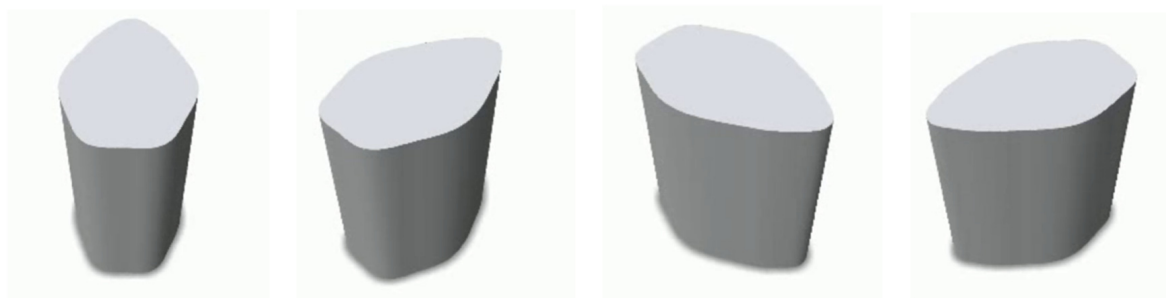


Figure 21. Appearance of Shape F when viewed from multiple perspectives.

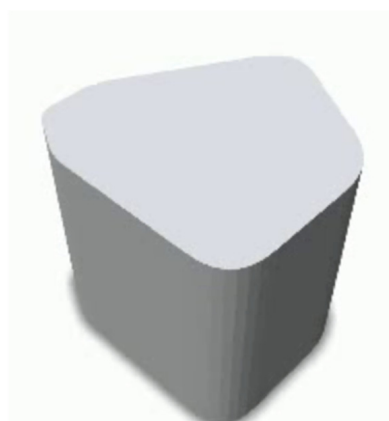


Figure 22. Perspective from which Shape D appears irregular.

■ Shapes for which the proposed index underestimates order

Figure 16 shows that the proposed index underestimated the order of Shapes C, E, G, and H. Figure 23 shows that these shapes share common characteristics, such as familiar shapes and mirror asymmetry in the yz -plane. Shapes such as Shapes G and H, which are basic geometric shapes such as equilateral triangles, and shapes such as Shape C, which has star-like configurations, are probably familiar and recognizable by the participants. Furthermore, Shape E, with its regular protrusions and a shape reminiscent of the letter 'W', is probably a familiar shape to the participants. Therefore, even if these shapes had mirror asymmetry in the yz -plane, the order of the sensory evaluation values was considered to be high. Consequently, it is suggested that the difference between the proposed index and sensory evaluation values is significant for these shapes and that the proposed index underestimates their order.

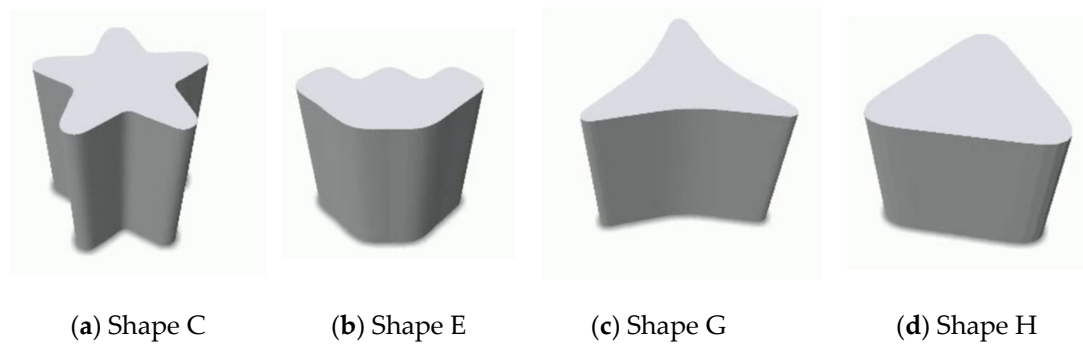


Figure 23. Shapes for which order is underestimated by the proposed index.

3.2.2. Rotated Shape

Figure 24 illustrates the relationship between the proposed index and the sensory evaluation of the order for various numbers of bins (integers ranging from 2 to 20) in rotated shapes. In this study, we set the center of mass of the shapes at the origin in xyz -space, and the shapes were oriented such that the rotation axis was aligned with the z -axis; we calculated seven proposed indices, such as the extruded shapes. Figure 24 shows that for all combinations of bin numbers, the coefficients of determination between the proposed indices and the sensory evaluation of order in rotated shapes are consistently below 0.1, indicating no correlation between the two. We now discuss the possible reasons for this observation.

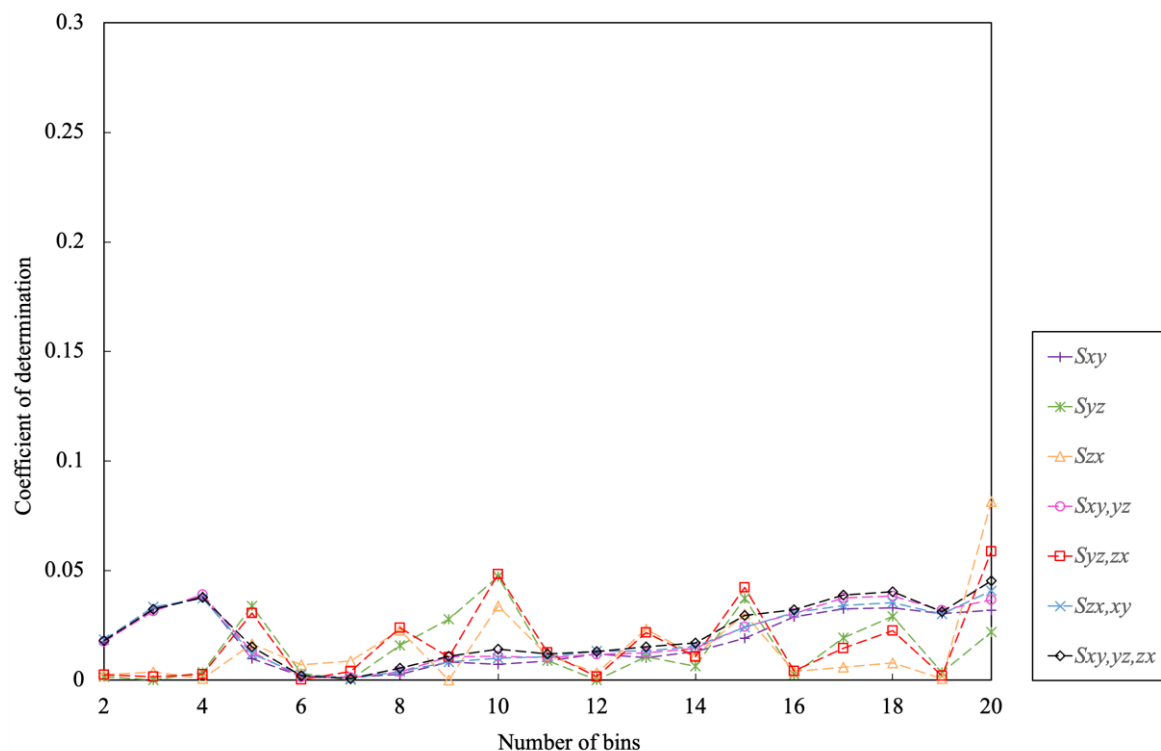


Figure 24. Relationship between the number of bins and coefficient of determination in rotated shapes.

The rotated shapes exhibited nearly perfect mirror symmetry with respect to the planes parallel to the rotation axis (yz -plane and zx -plane), resulting in the values of S_{yz} , S_{zx} , and $S_{yz,zx}$ being close to zero for all shapes. The slight deviations from zero are attributed to the noise introduced by the polygon equal-division process. Therefore, the coefficients of determination between the proposed indices for these planes and the sensory evaluation of the order are believed to be small. In contrast, planes perpendicular to the rotation

axis (xy -plane) have inherent mirror asymmetry, leading to variations in the values of S_{xy} depending on the shape. Consequently, a stronger correlation with the sensory evaluation of the order was expected. However, Figure 24 shows that the coefficient of determination remained small. The human perception of mirror symmetry of objects can explain this. Humans tend to detect and emphasize mirror symmetry with planes containing the vertical axis (planes parallel to the rotation axis in the case of rotated shapes) when perceiving mirror symmetry in things [44,46,56,57]. Therefore, it is likely that the participants did not consider mirror symmetry with planes perpendicular to the rotation axis (xy -plane) when evaluating the order of the rotated shapes. Therefore, the correlation between S_{xy} and the sensory evaluation values of the order is expected to be small. Furthermore, the high sensory evaluation values of order for all rotated shapes were considered to contribute to the overall lower coefficient of determination between the proposed indices and the sensory evaluation values of order. This may be explained by the fact that many items used in our daily lives have been made using a rotation process, originally with lathes and more recently with turning machining. Consequently, it is likely that the participants were familiar with and accustomed to rotated shapes. Additionally, the fact that the rotation axis used to create the rotated shapes was the same as that used to present the shapes in the experiment may be one of the reasons for these results. Because of the abovementioned characteristics of human symmetry perception, it is believed that the fact that all rotational shapes were perfectly mirror-symmetrical with respect to the plane containing the axis of rotation at the time of presentation made it difficult for variations in the sensory evaluation values to emerge among the shapes [38,40,62,63].

3.2.3. Vase Shape

First, we detail the results, and then we discuss our analysis of how the coefficient of determination vary with the number of segmented surfaces. Figure 25 illustrates the relationship between the proposed index and the sensory evaluation of the order in vase shapes for varying numbers of bins (integers ranging from 2 to 20). In this study, we set the center of mass of the shapes at the origin in xyz -space and oriented the shape such that the bottom of the vase lies parallel to the xy -plane, and we computed seven proposed indices, such as the extruded shapes. Figure 25 shows that the maximum coefficient of determination with the sensory evaluation values of order was achieved when the proposed index $S_{yz,zx}$ was calculated for bin number 14, resulting in a coefficient of determination of 0.66. Additionally, Figure 25 shows that the proposed indices considering mirror symmetry in the xy -plane ($S_{xy,yz}$, $S_{zx,xy}$, and $S_{xy,yz,zx}$) have a lower coefficient of determination with the sensory evaluation values of the order. This is because humans perceive mirror symmetry in objects. Humans are more likely to perceive and prioritize mirror symmetry in planes that include a vertical axis among all symmetrical planes [38,40,62,63]. Therefore, when evaluating the order of the vase shapes, the participants largely ignored mirror symmetry concerning the planes parallel to the bottom of the vase. Consequently, disregarding mirror symmetry in the xy -plane led to higher coefficient of determination with the order sensory evaluation scores. Furthermore, compared with the proposed indices considering mirror symmetry in the yz -plane or zx -plane (S_{yz} or S_{zx}), those considering mirror symmetry in both the yz - and zx -planes ($S_{yz,zx}$) achieved a larger coefficient of determination with sensory evaluation values of order. This is likely because humans evaluate the mirror symmetry of shapes from multiple angles, not just one [38–40,54]. Therefore, calculating the proposed indices by dividing the shapes into multiple planes resulted in a larger coefficient of determination with the sensory evaluation values of the order.

Next, we considered the index $S_{yz,zx}$, which exhibited the highest coefficient of determination among the seven proposed indices. We examined why the coefficient of determination varied with bin count, specifically for larger and smaller numbers of bins. In Figure 25, it is evident that the proposed index $S_{yz,zx}$ exhibits the smallest coefficient of determination when two bins are used. This decline shares the same causes as the proposed $S_{yz,zx}$ indices for the extruded shapes. Figure 25 also reveals that, similar to extruded

shapes, the coefficient of determination for vase shapes gets consistently larger for bin numbers greater than or equal to 6. Therefore, it can be inferred that six or more bins are necessary in this experiment.

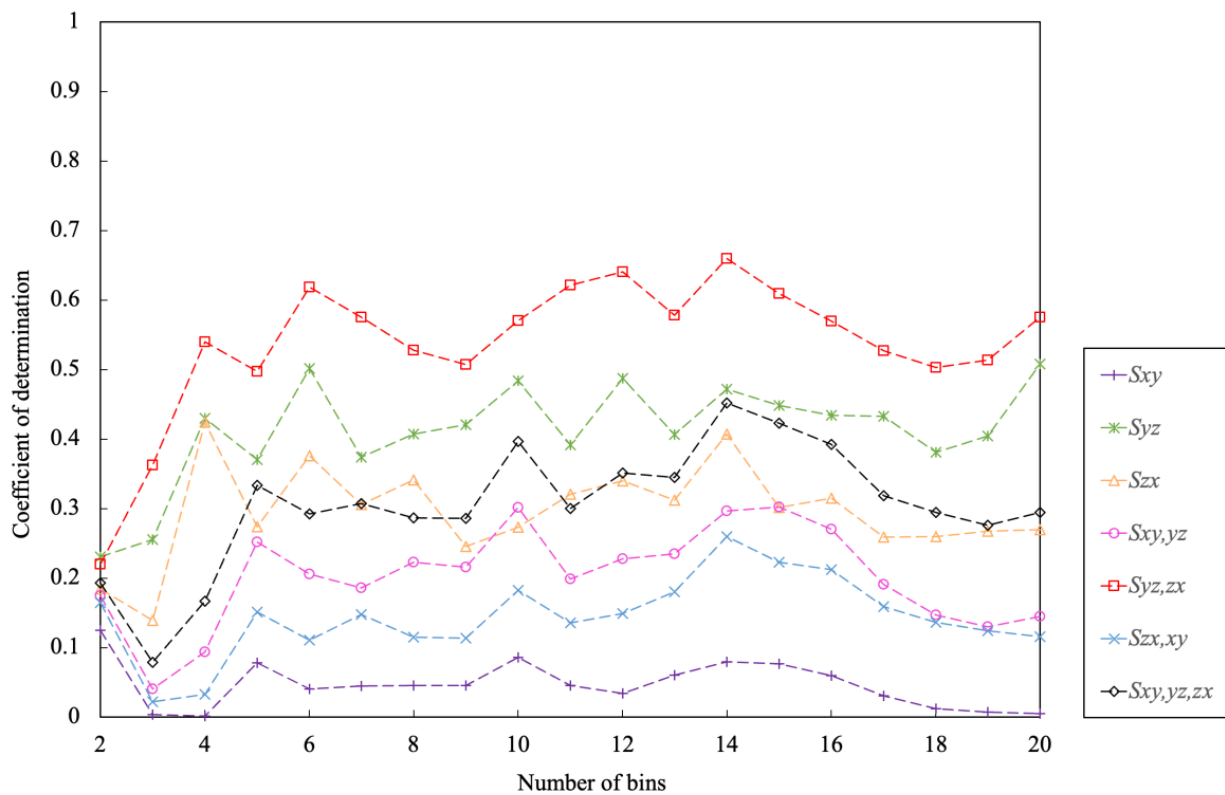


Figure 25. Relationship between the number of bins and coefficient of determination in vase shapes.

Therefore, from bin numbers 6–20, Figure 26a,b presents scatter plots of the proposed index and sensory evaluation values for the cases with the minimum coefficient of determination in bin number 9 and maximum coefficient of determination in bin number 14, respectively. It is evident from the two scatter plots that as the bin number changes from 9 to 14, the proposed index values for Shapes I and J become smaller compared to other shapes, approaching the regression line. This suggests that the coefficient of determination increased significantly for bin 14. The contour plots of the curvature and histograms of the curvature distributions for Shapes I and J are shown in Figures 27–32. Figures 27 and 30 show contour plots and histograms in bin 9 for Shapes I and J, respectively. In addition, Figures 28 and 31 show contour plots and histograms at bin 14 for Shapes I and J, respectively. In Figures 27 and 28, as well as Figures 30 and 31, it can be observed that for bin 14, there is a significant curvature (highlighted in red in the contour plots) in the part of the shape corresponding to the handle, which is not distinguishable at bin 9. This observation is further supported by the histograms in Figures 27 and 28, as well as Figures 30 and 31, where for both shapes, a new distribution appears in the second bin from the left when the bin number changes from 9 to 14. This suggests that for bin 14, there is a significant difference in the curvature distribution across various parts of the shape when compared to bin 9, resulting in the proposed index values becoming smaller (i.e., closer to the sensory evaluation values). Therefore, it is believed that the coefficient of determination is larger for bin 14.

Furthermore, scatter plots of the sensory evaluation values of the proposed index and order for the number of bins with the largest coefficient of determination (14) and the number of bins with the largest coefficient of determination (20) in the extruded shape are shown in Figures 26b and 26c, respectively. The blue-colored plots (Shapes I and J) are discussed below. The two scatter plots show that as the bin number changes from 14 to 20,

the values of the proposed index for Shapes I and J become smaller compared with the other shapes and move farther away from the regression line. Therefore, it is believed that the coefficient of determination decreases in the case of 20 bins. Contour plots of the curvature in shape and histograms for each part are shown in Figures 27–32 for each number of bins. Figures 28 and 31 show contour plots and histograms at bin 14 for Shapes I and J, respectively. In addition, Figures 29 and 32 show contour plots and histograms at bin 20 for Shapes I and J, respectively. These figures indicate that for 14 bins, the curvature around the handle area is not distinguishable from the curvature of the other surfaces, whereas for 20 bins, the curvatures of the other surfaces become more distinguishable. Consequently, for 20 bins, there is a larger difference in the curvature distribution across various parts of the shape, leading to higher values for the proposed index. However, Shapes I and J are asymmetric shapes with a ‘handle’ on one side, which can be recognized as a single function in a vase. Therefore, the subjects did not significantly reflect the asymmetry of the shape due to the presence of the ‘handle’ in the evaluation of the order. This resulted in the order of sensory evaluation values of these shapes being moderate. When the number of bins was increased to 20, the correlation between the proposed index and the sensory evaluation values of the order weakened, leading to a smaller overall coefficient of determination for the vase shape.

Finally, we discuss the proposed index $S_{yz,zx}$ (bin number 14), which exhibits the highest coefficient of determination with the order of sensory evaluation values. Figure 33 shows the scatter plot of $S_{yz,zx}$ (bin number 14) and the order of the sensory evaluation values. The yellow-colored plots (Shapes J, K, L, M and N) are discussed below. Figure 33 shows a strong correlation, with a coefficient of determination of 0.66 for the vase shape, indicating a robust relationship between $S_{yz,zx}$ (bin number 14) and the sensory evaluation values of the order. We consider shapes for which there is a significant difference between the proposed index and the sensory evaluation values.

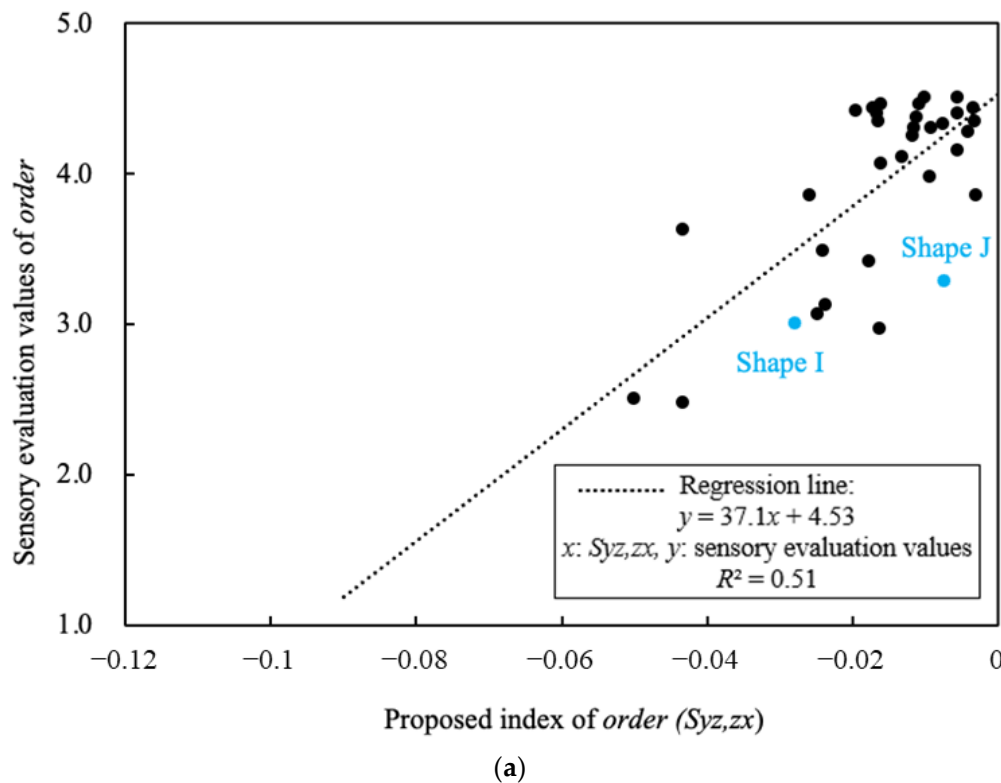
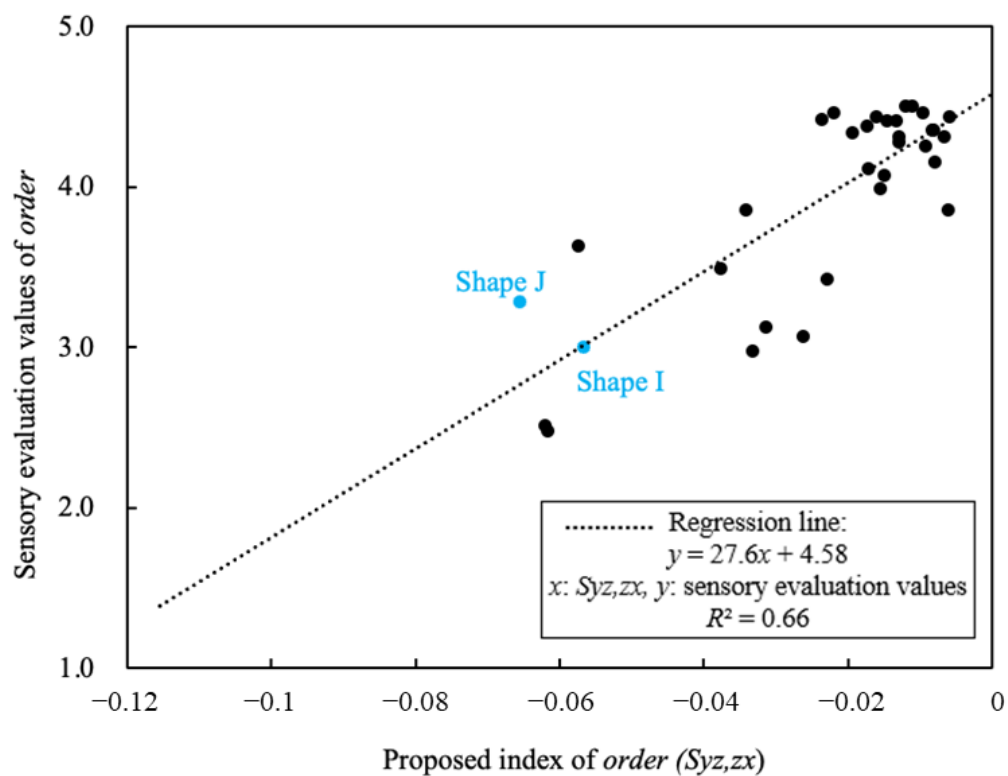
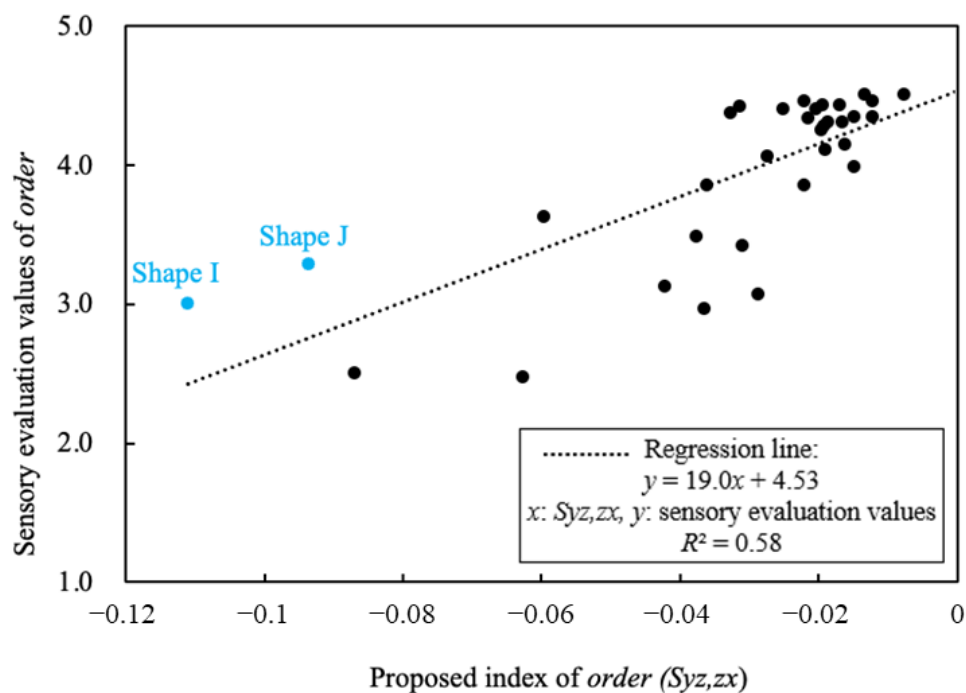


Figure 26. Cont.



(b)



(c)

Figure 26. Relationship between the proposed index $S_{yz,zx}$ and sensory evaluation values of ‘order’ in (a) bin number 9, (b) bin number 14, and (c) bin number 20.

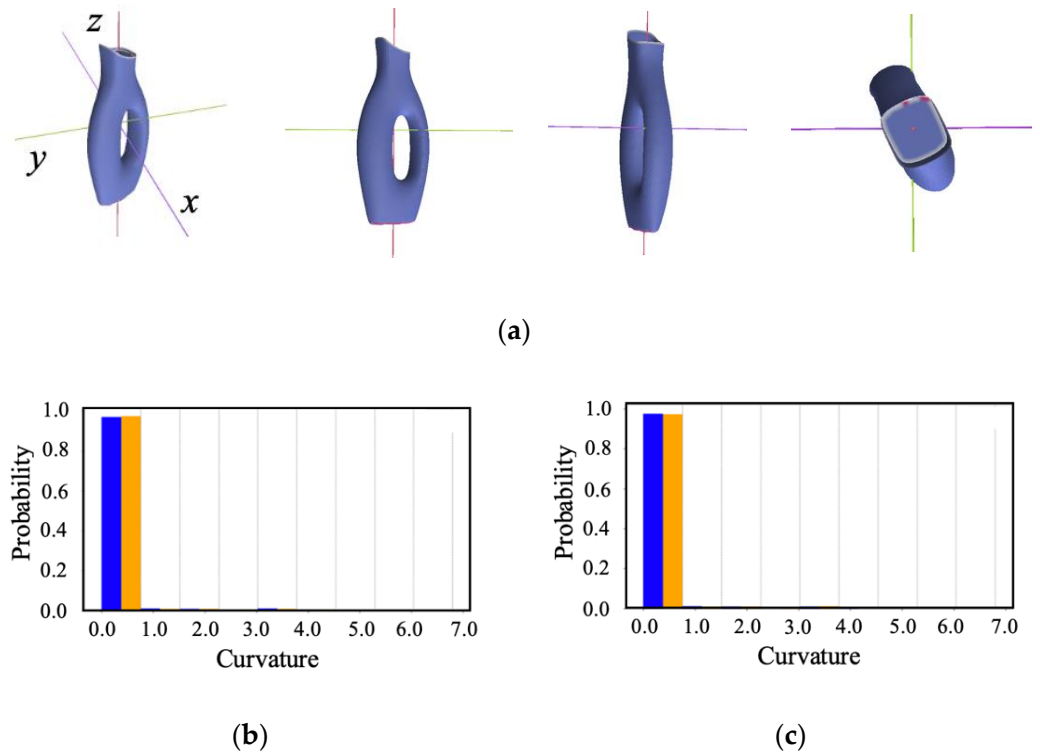


Figure 27. Contour plots and curvature distributions in Shape I in bin number 9: (a) contour plots from different perspectives, (b) curvature distribution of each part (blue and orange) obtained for the yz -plane, and (c) curvature distribution of each part (blue and orange) obtained for the zx -plane.

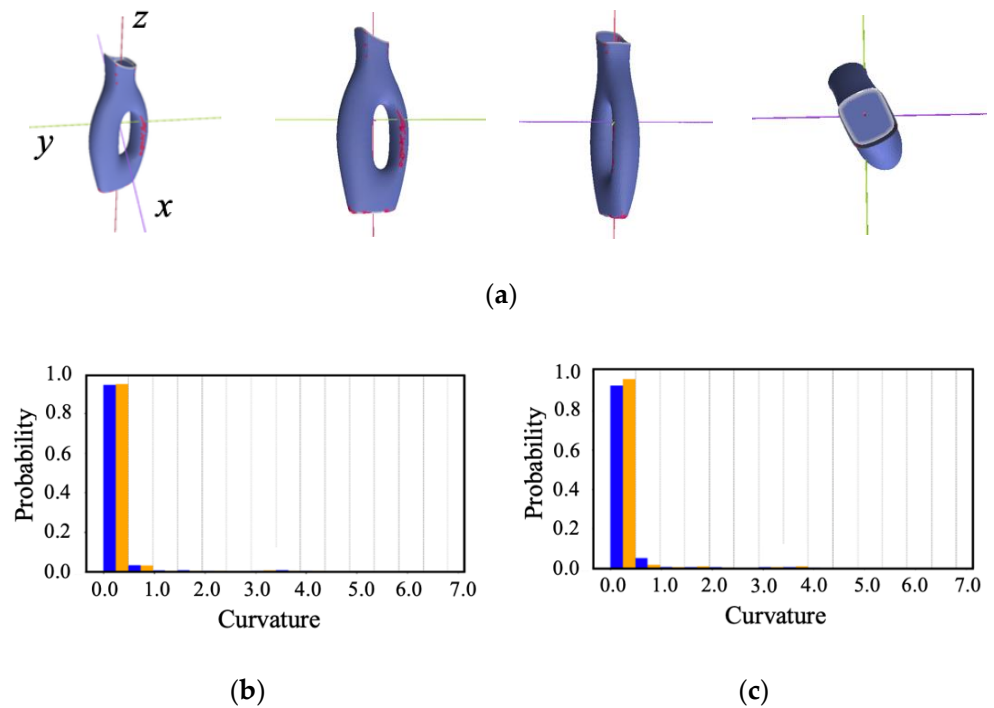


Figure 28. Contour plots and curvature distributions in Shape I in bin number 14: (a) contour plots from different perspectives, (b) curvature distribution of each part (blue and orange) obtained for the yz -plane, and (c) curvature distribution of each part (blue and orange) obtained for the zx -plane.

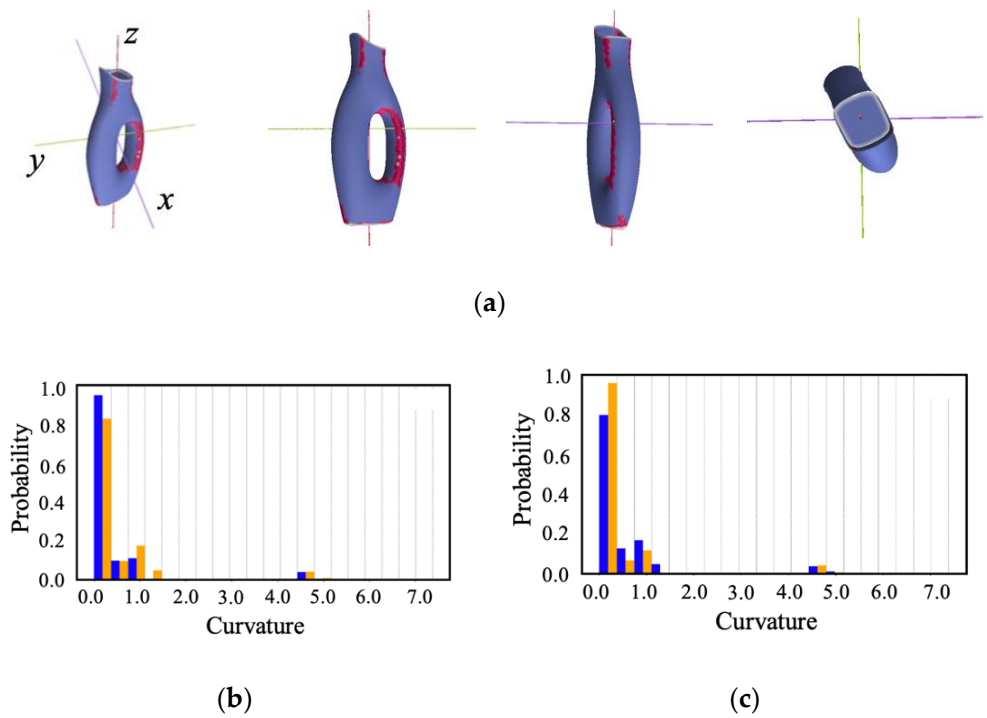


Figure 29. Contour plots and curvature distributions in Shape I in bin number 20: (a) contour plots from different perspectives, (b) curvature distribution of each part (blue and orange) obtained for the yz -plane, and (c) curvature distribution of each part (blue and orange) obtained for the zx -plane.

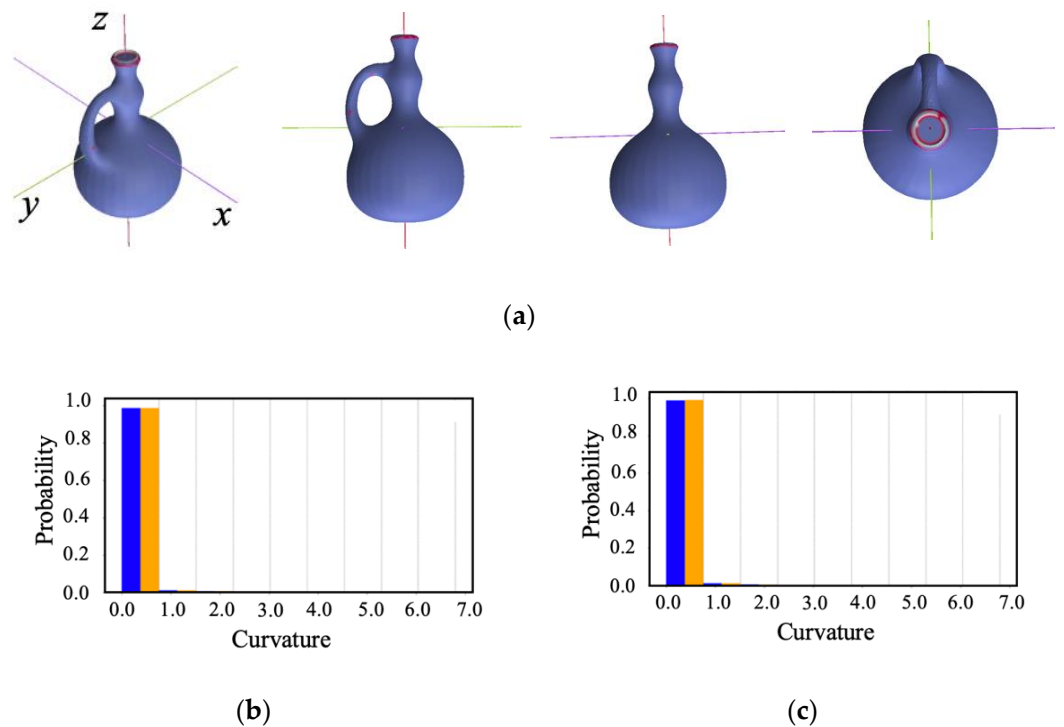


Figure 30. Contour plots and curvature distributions in Shape J in bin number 9: (a) contour plots from different perspectives, (b) curvature distribution of each part (blue and orange) obtained for the yz -plane, and (c) curvature distribution of each part (blue and orange) obtained for the zx -plane.

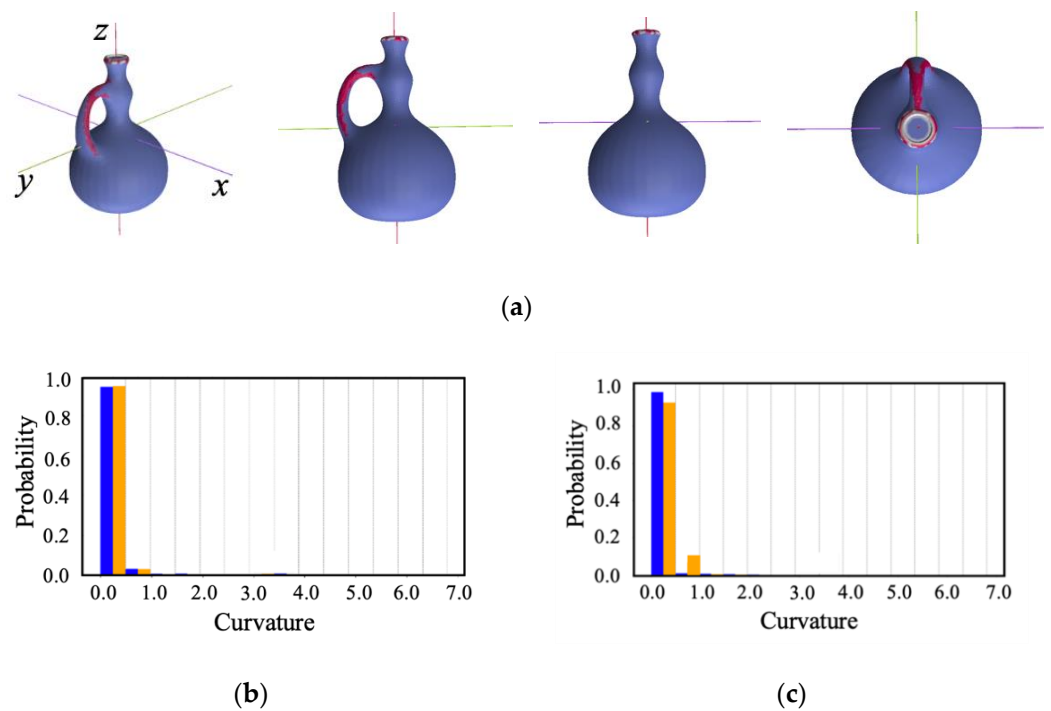


Figure 31. Contour plots and curvature distributions in Shape J in bin number 14: (a) contour plots from different perspectives, (b) curvature distribution of each part (blue and orange) obtained for the yz -plane, and (c) curvature distribution of each part (blue and orange) obtained for the zx -plane.

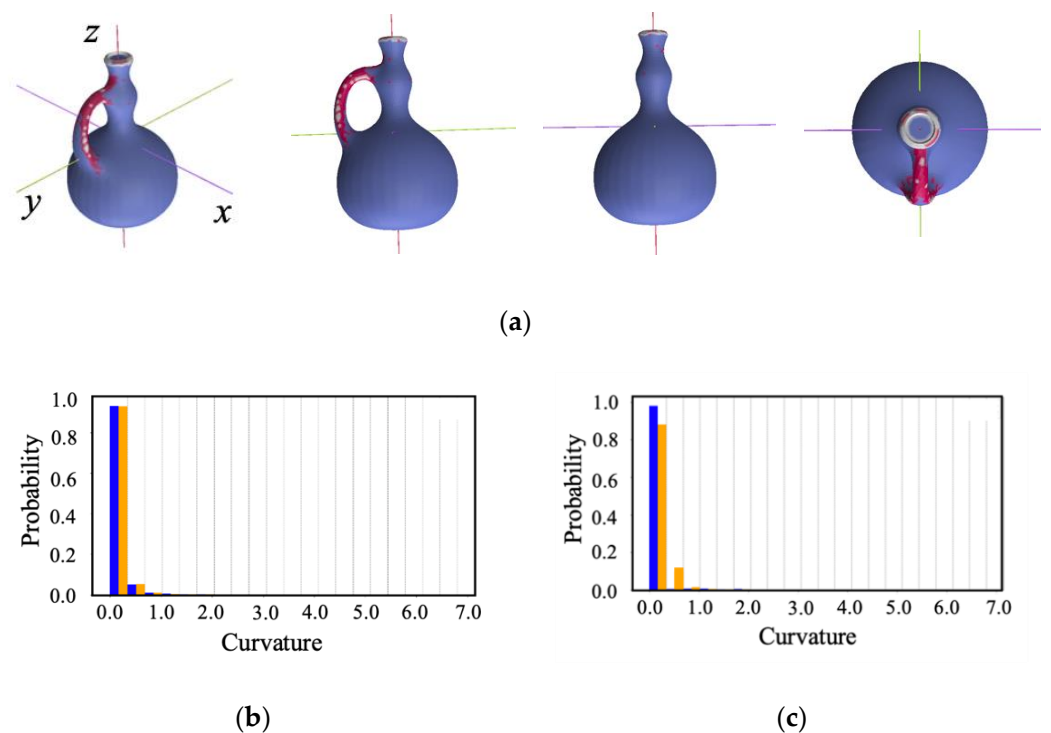


Figure 32. Contour plots and curvature distributions in Shape J in bin number 20: (a) contour plots from different perspectives, (b) curvature distribution of each part (blue and orange) obtained for the yz -plane, and (c) curvature distribution of each part (blue and orange) obtained for the zx -plane.

■ Shapes for which the proposed index overestimates order

Figure 33 shows that the proposed index overestimates the order for Shapes K, L, and M. Figures 34–36 depict the contour plots and histograms of the curvature for each

shape. Among these, Shape K exhibits irregular ‘undulations’ on its surface, while both Shapes L and M have left-right asymmetric ‘openings’. Figure 33 indicates that the sensory evaluation values for the order of these shapes were low. However, as is evident from the contour plots and histograms in Figures 34–36, when the shapes were divided in the zx -plane, the curvature distributions in each divided part were nearly identical. Similarly, when divided in the yz -plane, there was little variation in the curvature distribution among the divided parts. Consequently, it is safe to conclude that the proposed index values are approximately the average (rather than near the minimum) in these cases. Therefore, we suggest that the proposed index overestimates order.

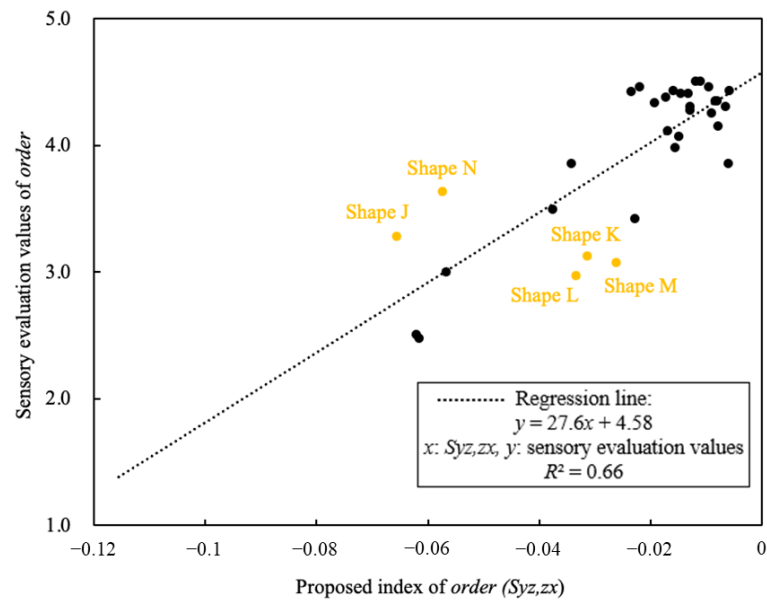


Figure 33. Relationship between the proposed index $S_{yz,zx}$ and sensory evaluation values of ‘order’ in bin number 14.

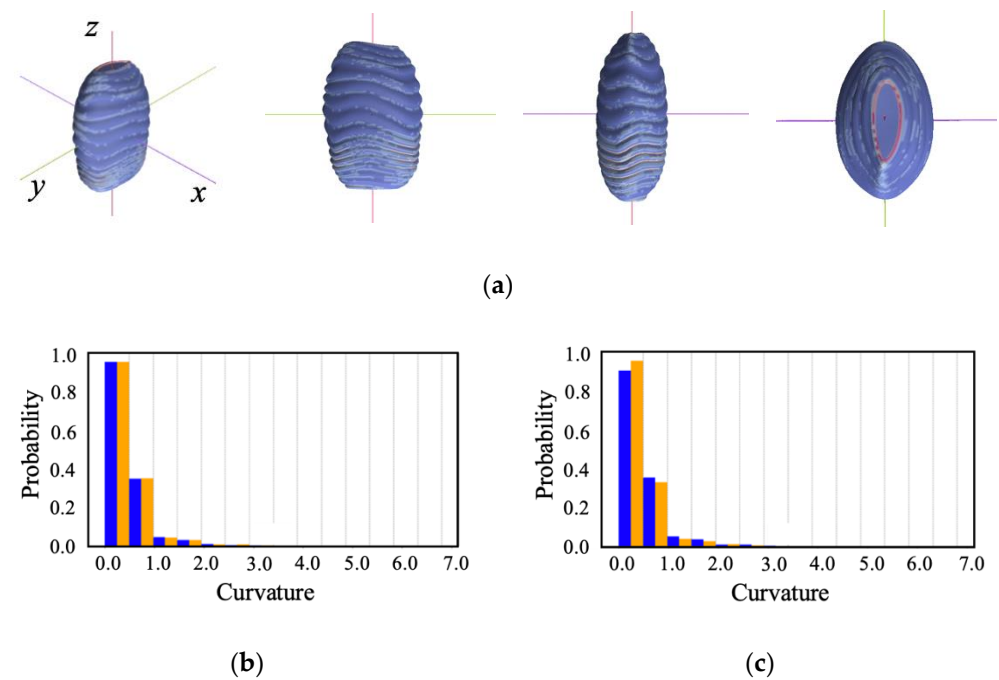


Figure 34. Contour plots and curvature distributions in Shape K: (a) contour plots from different perspectives, (b) curvature distribution of each part (blue and orange) obtained for the yz -plane, and (c) curvature distribution of each part (blue and orange) obtained for the zx -plane.

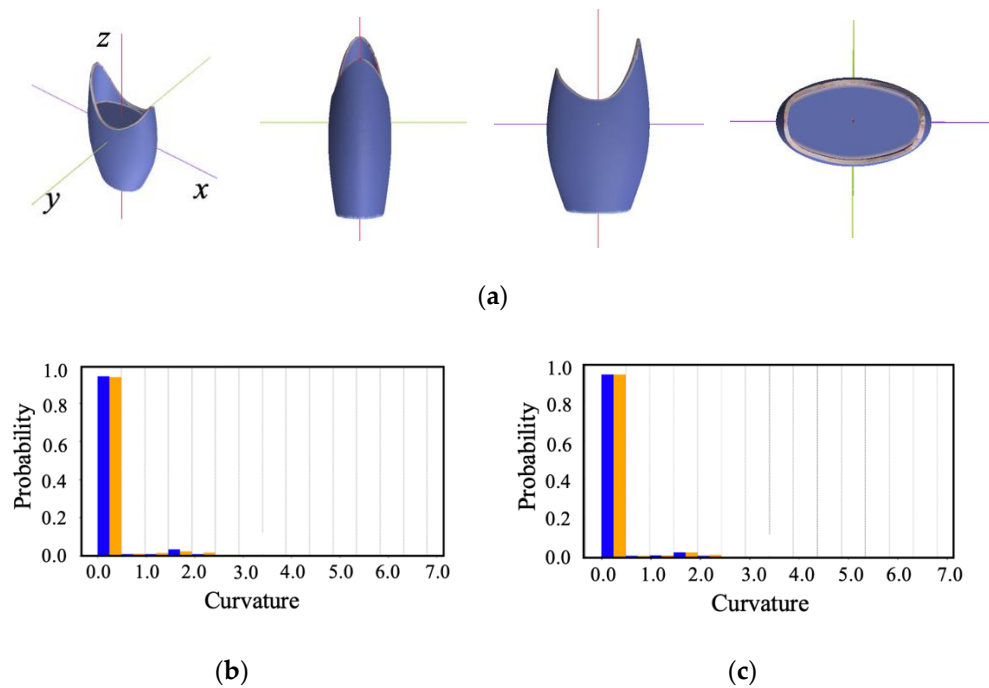


Figure 35. Contour plots and curvature distributions in Shape L: (a) contour plots from different perspectives, (b) curvature distribution of each part (blue and orange) obtained for the yz -plane, and (c) curvature distribution of each part (blue and orange) obtained for the zx -plane.

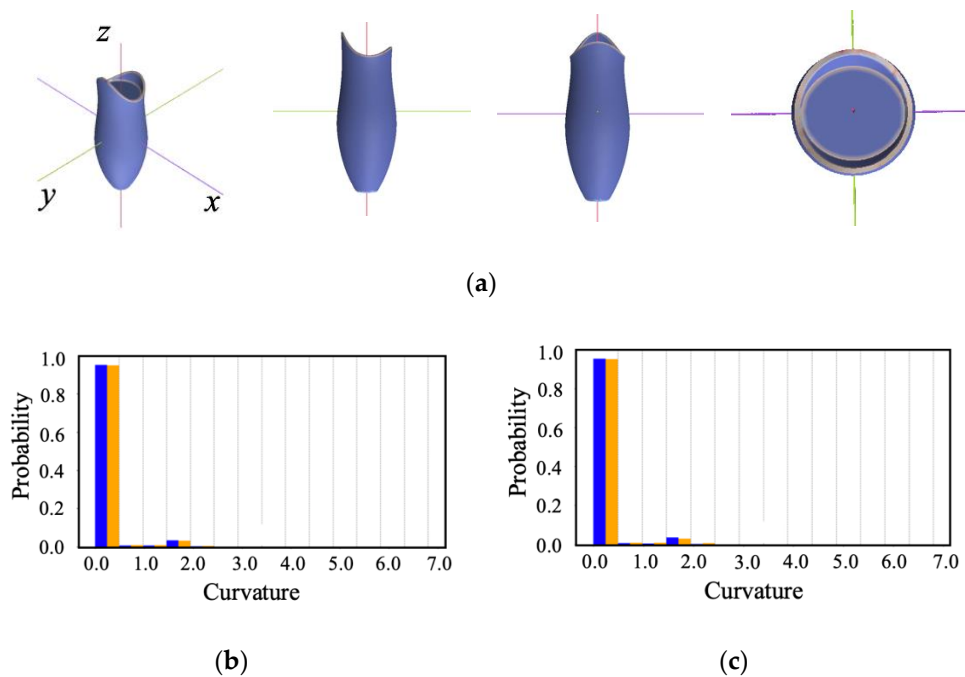


Figure 36. Contour plots and curvature distributions in Shape M: (a) contour plots from different perspectives, (b) curvature distribution of each part (blue and orange) obtained for the yz -plane, and (c) curvature distribution of each part (blue and orange) obtained for the zx -plane.

■ Shapes for which the proposed index underestimates order

Figure 33 shows that the proposed index underestimates the order for Shapes N and J. For each shape, the contour plots of the shape curvature and histograms of the curvature for each part are shown in Figures 37 and 38. Shape N is a shape where the ‘openings’ part functions convincingly as a ‘pouring spout’. For Shape J, the presence of a ‘handle’

was functionally acceptable for a vase. However, these shapes exhibit significant changes in curvature distribution among the divided parts due to the asymmetry caused by the ‘mouth’ and ‘handle’ when divided in the yz -plane, as evident from the contour plots and histograms in Figures 37 and 38. Consequently, the proposed index values for the same shapes increase. Therefore, we suggest that the proposed index underestimates the order.

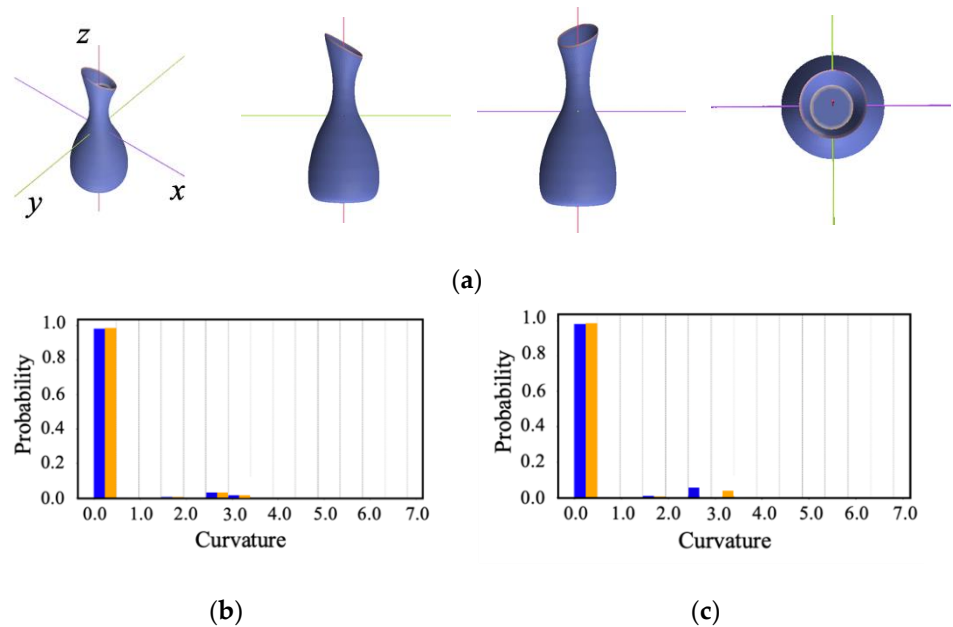


Figure 37. Contour plots and curvature distributions in Shape N: (a) contour plots from different perspectives, (b) curvature distribution of each part (blue and orange) obtained for the yz -plane, and (c) curvature distribution of each part (blue and orange) obtained for the zx -plane.

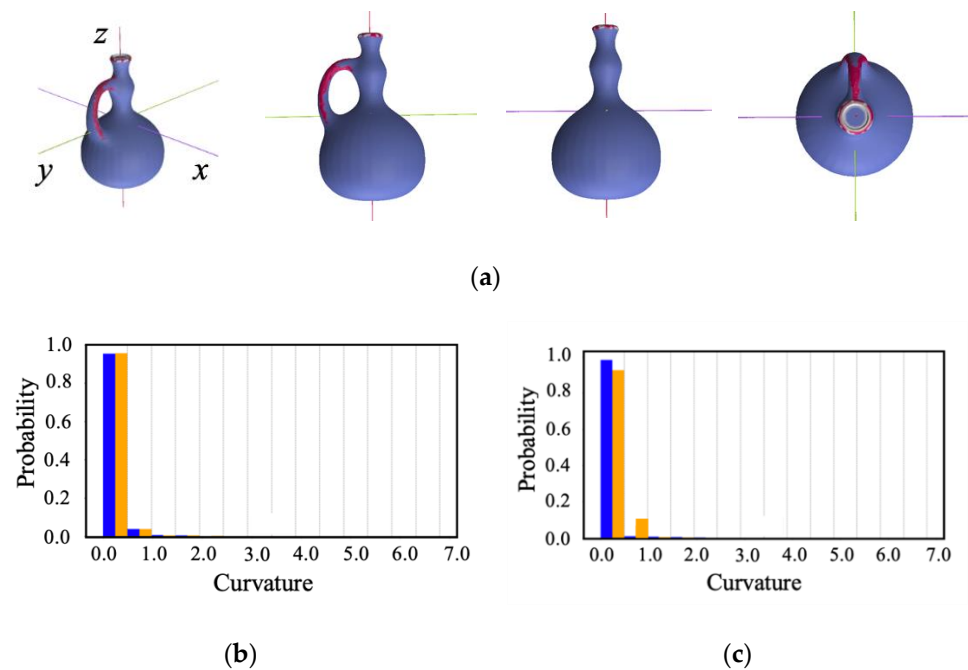


Figure 38. Contour plots and curvature distributions in Shape J: (a) contour plots from different perspectives, (b) curvature distribution of each part (blue and orange) obtained for the yz -plane, and (c) curvature distribution of each part (blue and orange) obtained for the zx -plane.

4. Conclusions

In this study, we initially computed the Casorati curvature of three-dimensional shapes and used it to quantify the degree of ‘mirror symmetry’ in these shapes. We derived a quantification index for order in three-dimensional shapes. The proposed index allows for the assessment with traditional mirror symmetry in different shapes, even those with holes, which was challenging. Sensory evaluation experiments were performed to confirm the effectiveness of the proposed index. Specifically, these experiments were performed on three distinct shapes: extruded, rotated, and vase shaped. For the rotation shapes, the coefficient of determination between the proposed index and the sensory evaluation values was 0.1 or lower. However, for both the extrusion and vase shapes, the coefficient of determination between the proposed index and the sensory evaluation values were higher at 0.36 and 0.66, respectively, supporting the effectiveness of our proposed index. The application of this index to the aesthetic evaluation of shapes in generative design is expected to streamline product design processes, leading to time and cost savings.

For future tasks, there are several approaches to consider. First, it may be beneficial to re-evaluate the method of presenting shapes in experiments, considering the nuances of human symmetry perception, particularly for rotational shapes that did not yield significant results in this study. Specifically, the shapes can be presented by rotating them around an axis other than the vertical axis. Second, conducting sensory evaluation experiments with additional sample shapes to validate the utility of the proposed index is another avenue of exploration. The sample shapes that could be used include a 2D triangular shape [54], a three-dimensional humidifier [23], a jawbone [44], and a bottle shape [37], which have been used in some previous studies on order and symmetry of three-dimensional shapes. Lastly, combining the quantification index for ‘order’ proposed in this study with quantification indices for ‘complexity’ could lead to the quantification of ‘aesthetic preferences’ in three-dimensional shapes.

Author Contributions: Conceptualization, T.S.; Methodology, T.S.; Software, T.S. and M.O.; Validation, T.S. and Y.I.; Formal Analysis, T.S.; Investigation, T.S. and Y.I.; Resources, T.S.; Data Curation, T.S., M.O. and Y.I.; Writing—Original Draft Preparation, T.S.; Writing—Review and Editing, T.S. and T.K.; Visualization, T.S.; Supervision, T.K.; Project Administration, T.K.; Funding Acquisition, T.K. All authors have read and agreed to the published version of the manuscript.

Funding: This study was partly supported by Japan Society for the Promotion of Science (JSPS) KAKENHI Grant-Number 23K11746 and 21H03528.

Informed Consent Statement: This study was approved by the institutional review board, and written informed consent was obtained from the participants.

Data Availability Statement: The data from this research are partly available to interested parties upon request to the corresponding author.

Acknowledgments: The authors would like to thank K. Matsuyama, as well as R. Noji for programming assistance. We also thank all participants of the sensory evaluation experiment.

Conflicts of Interest: The authors declare no conflicts of interest.

Appendix A

The following describes the calculation of the Casorati curvature in a polygon model. The curvature calculation method is described for the polygonal mesh in Figure A1. Where v_i is the vertex whose curvature is to be calculated, v_{ik} ($k = 1, 2, \dots, n_i$) are vertices adjacent to vertex v_i , f_{ik} ($k = 1, 2, \dots, n_i$) are polygons with v_i as a vertex, and $a_{ik} = \angle (v_{ik}, v_i, v_{i(k+1)})$ is the angle of f_{ik} at vertex v_i .

1. First, we calculate the Gaussian curvature directly from the polygon model. Using Gauss-Bonnet’s law [64], the Gaussian curvature K_i at i th vertex v_i can be expressed as follows, where A is the sum of the areas of the polygons around the vertex v_i .

$$K_i = \frac{2\pi - \sum_{k=1}^{n_i} \alpha_{ik}}{\frac{1}{3}A} \tag{A1}$$

2. Second, the mean curvature is obtained directly from the polygon model. Using Gauss-Bonnet’s law and paraboloid fitting [64], the mean curvature H_i at i th vertex v_i is calculated as follows, where e_{ik} is the distance between vertex v_i and its neighbor vertices $v_{ik} (k = 1, 2, \dots, n_i)$ and β_{ik} is the angle between adjacent polygons.

$$H_i = \frac{\frac{1}{4} \sum_{k=1}^{n_i} \|e_{ik}\| \beta_{ik}}{\frac{1}{3}A} \tag{A2}$$

3. Third, using the results of 1 and 2, the principal curvatures k_1 and k_2 are calculated. The mean curvature H is defined as the mean value of the principal curvatures, and the Gaussian curvature K is defined as the product of the principal curvatures. Therefore, the principal curvatures k_1 and k_2 can be calculated by combining the two equations. When the maximum principal curvature is k_1 and the minimum principal curvature is k_2 , both are expressed by the following equations:

$$k_1 = H + \sqrt{H^2 - K} \tag{A3}$$

$$k_2 = H - \sqrt{H^2 - K} \tag{A4}$$

4. Finally, the Casorati curvature was calculated using k_1 and k_2 . The Casorati curvature is calculated as follows:

$$C_c = \frac{\sqrt{k_1^2 + k_2^2}}{2} \tag{A5}$$

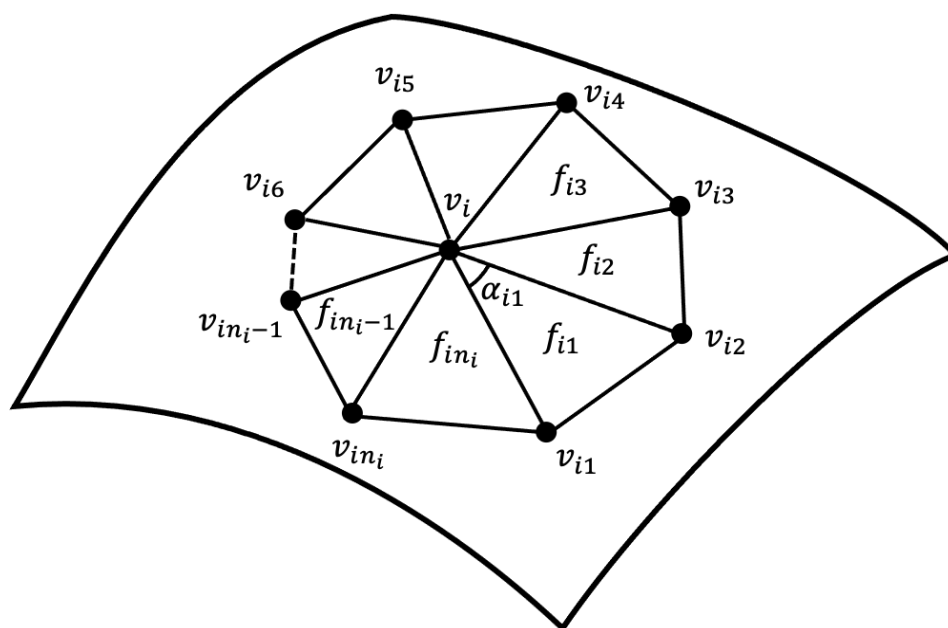


Figure A1. Polygons around vertex v_i .

References

1. Byrne, J.; Philip, C.; Anthony, B.; Michael, O. Evolving Parametric Aircraft Models for Design Exploration and Optimisation. *Neurocomputing* 2014, 142, 39–47. [CrossRef]

2. Cgasee, S.C. Generative design tools for novice designers: Issues for selection. *Autom. Constr.* **2005**, *14*, 689–698.
3. Olocher, J.; Panesar, A. Review on design and structural optimisation in additive manufacturing: Towards next-generation lightweight structures. *Mater. Des.* **2019**, *183*, 108–164.
4. Singh, V.; Gu, N. Towards an integrated generative design framework. *Des. Stud.* **2012**, *33*, 185–207. [[CrossRef](#)]
5. Shea, K.; Aish, R.; Gourtovavia, M. Towards integrated performance-driven generative design tools. *Autom. Constr.* **2005**, *14*, 253–264. [[CrossRef](#)]
6. Yavuz, A.Ö.; Sahar, S. A Practice Upon Transformation of Creative Data at Architectural Basic Design Education. *Procedia Soc. Behav. Sci.* **2014**, *143*, 389–393. [[CrossRef](#)]
7. Honda, S.; Yanagisawa, H.; Kato, T. Aesthetic shape generation system based on novelty and complexity. *J. Eng. Des.* **2022**, *33*, 1016–1035. [[CrossRef](#)]
8. Krish, S. A practical generative design method. *Comput. Aided Des.* **2011**, *43*, 88–100. [[CrossRef](#)]
9. Lin, M.H.; Lee, C.L. An Experimental Study for Applying Generative Design to Electronic Consumer Products. *Int. Conf. Des. User Exp. Usability* **2013**, *8015*, 392–401.
10. Jordan, P. *Designing Pleasurable Products. An Introduction to the New Human Factors*; CRC Press: London, UK, 2000.
11. Tiger, L. *The Pursuit of Pleasure*; Little Brown: Boston, MA, USA, 1992.
12. Perez, M.M.; Ahmed-Kristensen, S.; Brockhoff, P.B.; Yanagisawa, H. Investigating the influence of product perception and geometric features. *Res. Eng. Des.* **2017**, *28*, 357–379. [[CrossRef](#)]
13. Arnheim, R. *Toward a Psychology of Art*; University of California Press: Berkeley, CA, USA, 1966.
14. Eysenck, H.J. The experimental study of the good Gestalt. *Psychol. Rev.* **1942**, *49*, 344–364. [[CrossRef](#)]
15. Garner, W.R. *The Processing of Information Structure*; Psychology Press: New York, NY, USA, 1975.
16. Gombrich, E.H. *Art and Illusion: A Study in the Psychology of Pictorial Representation*; Pantheon: Roma, Italy, 1960.
17. Gombrich, E.H. *The Sense of Order: A Study in the Psychology of Decorative Art*; Cornell University Press: New York, NY, USA, 1979.
18. Solso, L. *Cognition and the Visual Arts*; MIT Press: Cambridge, MA, USA, 1994.
19. Berlyne, D.E. *Aesthetics and Psychobiology*; Appleton Century Crofts: New York, NY, USA, 1971.
20. Birkhoff, G.D. *Aesthetic Measure*; Harvard University Press: Cambridge, UK, 1933.
21. Boselie, F.; Leeuwenberg, E. Birkhoff revisited: Beauty as a function of effect and means. *Am. J. Psychol.* **1985**, *98*, 1–39. [[CrossRef](#)]
22. Eibl-Eibesfeldt, I. The biological foundation of aesthetics. In *Beauty and the Brain*; Rentschler, I., Herzberger, B., Epstein, D., Eds.; Springer: Basel, Switzerland, 1988; pp. 29–68.
23. Kato, T.; Matsumoto, T. Morphological evaluation of closed planar curves and its application to aesthetic evaluation. *Graph. Models* **2020**, *109*, 101064. [[CrossRef](#)]
24. Moles, A. *Information Theory and Esthetic Perception*; University of Illinois Press: Champaign, IL, USA, 1969.
25. Eysenck, H.J. The empirical determination of an aesthetic formula. *Psychol. Rev.* **1941**, *48*, 83–92. [[CrossRef](#)]
26. Vitz, P.C. Preference for different amounts of visual complexity. *Behav. Sci.* **1966**, *11*, 105–114. [[CrossRef](#)]
27. Wang, D.; Belyaev, A.; Saleem, W.; Seidel, H. *Shape Complexity and Image Similarity*; Max-Planck-Institut für Informatik: Saarbrücken, Germany, 2008.
28. Saleem, W.; Belyaev, A.; Wang, D.; Seibel, H. On visual complexity of 3d shapes. *Comput. Graph.* **2011**, *35*, 580–585. [[CrossRef](#)]
29. Farin, G.; Rein, G.; Sapidis, N.; Worsey, A.J. Fairing cubic B-spline curves. *Comput. Aided. Geom. Des.* **1987**, *4*, 91–103. [[CrossRef](#)]
30. Sukumar, S.; Page, D.; Koschan, A.F.; Roui-Abidi, B.; Abidi, M. Shape analysis algorithm based on information theory. In Proceedings of the 2003 International Conference on Image Processing, Barcelona, Spain, 14–17 September 2003; pp. 1–229.
31. Matsumoto, T.; Sato, K.; Matsuoka, Y.; Kato, T. Quantification of ‘Complexity’ in curved surface shape using total absolute curvature. *Comput. Graph.* **2019**, *78*, 108–115. [[CrossRef](#)]
32. Okano, A.; Matsumoto, T.; Kato, T. Gaussian Curvature Entropy for Curved Surface Shape Generation. *Entropy* **2020**, *22*, 353. [[CrossRef](#)]
33. Matsuyama, K.; Shimizu, T.; Kato, T. Systematic Classification of Curvature and Feature Descriptor of 3D Shape and Its Application to ‘Complexity’ Quantification Methods. *Entropy* **2023**, *25*, 624. [[CrossRef](#)]
34. Sasaki, H.; Kato, T.; Yanagisawa, H. Quantification of “novelty” based on free-energy principle and its application for “aesthetic liking” for industrial products. *Res. Eng. Des.* **2023**, *35*, 21–41. [[CrossRef](#)]
35. Lu, P.; Shih-Wen, H.; Fan, W. A Product Shape Design and Evaluation Model Based on Morphology Preference and Macroscopic Shape Information. *Entropy* **2021**, *23*, 639. [[CrossRef](#)]
36. Lugo, J.E.; Valencia-Romero, A. Part-worth utilities of Gestalt principle for product esthetics: A case study of a bottle silhouette. *J. Mech. Des.* **2016**, *138*, 81–102.
37. Valencia-Romero, A.; Lugo, J.E. Quantification of Symmetry, Parallelism, and Continuity as Continuous Design Variables for Three-Dimensional Product Representations. In Proceedings of the ASME International Design Engineering Technical Conferences and Computers and Information in Engineering Conference, Charlotte, NC, USA, 21–24 August 2016.
38. Wagemans, J. Characteristics and models of human symmetry detection. *Trends Cogn. Sci.* **1997**, *1*, 346–352. [[CrossRef](#)]
39. Palmer, S.E.; Hemenway, K. Orientation and symmetry: Effects of multiple, rotational, and near symmetries. *J. Exp. Psychol. Hum. Percept Perform.* **1978**, *4*, 691–702. [[CrossRef](#)]
40. Royer, F.L. Detection of symmetry. *J. Exp. Psychol. Hum. Percept Perform.* **1981**, *7*, 1186–1210. [[CrossRef](#)]

41. Makin, A.D.J.; Rampone, G.; Pecchinenda, A.; Bertamini, M. Electrophysiological responses to visuospatial regularity. *Psychophysiology* **2013**, *50*, 1045–1056. [[CrossRef](#)]
42. Makin, A.D.J.; Rampone, G.; Wright, A.; Martinovic, J.; Bertamini, M. Visual symmetry in objects and gaps. *J. Vis.* **2014**, *14*, 12. [[CrossRef](#)]
43. Kazhdan, M.; Chazelle, B.; Dobkin, D.; Funkhouser, T.; Rusinkiewicz, S. A reflective symmetry descriptor for 3D models. *Algorithmica* **2003**, *38*, 201–225. [[CrossRef](#)]
44. Lin, Y.C.; Fang, J.J. Voxel-based, image source-independent 3D asymmetry quantification in the maxillofacial region. *Adv. Mater. Res.* **2012**, *452–453*, 165–169. [[CrossRef](#)]
45. Tuzikov, A.V.; Colliot, O.; Bloch, I. Evaluation of the symmetry plane in 3D MR brain images. *Pattern Recogn. Lett.* **2003**, *24*, 2219–2233. [[CrossRef](#)]
46. Ardekani, B.A.; Kershaw, J.; Braun, M.; Kanno, I. Automatic detection of the mid-sagittal plane in 3-D brain images. *IEEE Trans. Med. Imaging* **1997**, *16*, 947–952. [[CrossRef](#)] [[PubMed](#)]
47. Prima, S.; Commowick, O. Using bilateral symmetry to improve non-local means denoising of MR brain images. In Proceedings of the 2013 IEEE 10th International Symposium on Biomedical Imaging (ISBI), San Francisco, CA, USA, 7–11 April 2013; pp. 1231–1234.
48. Wong, T.Y.; Fang, J.J.; Wu, T.C. A novel method of quantifying facial asymmetry. *Int. Congr. Ser.* **2005**, *1281*, 1223–1226.
49. Antonelli, M.; Beccari, C.V.; Casciola, G.; Ciarloni, R. Subdivision surfaces integrated in a CAD system. *Comput. Aided Des.* **2013**, *45*, 1294–1305. [[CrossRef](#)]
50. Ma, W. Subdivision surfaces for CAD—An overview. *Comput. Aided Des.* **2004**, *37*, 693–709. [[CrossRef](#)]
51. Marais, P.; Guillemaud, R.; Sakuma, M.; Zisserman, A.; Brady, M. Visualising cerebral asymmetry. In Proceedings of the 4th International Conference on Visualization in Biomedical Computing (VBC'96), London, UK, 22–25 September 1996; pp. 411–416.
52. Lo, C.H. Application of aesthetic principles to the study of consumer preference models for vase forms. *Appl. Sci.* **2018**, *8*, 1199. [[CrossRef](#)]
53. Jan, J.; Koenderink; Andrea, J. Surface shape and curvature scales. *Image Vis. Comput.* **1992**, *10*, 262–8856.
54. Wenderoth, P. The salience of vertical symmetry. *Perception* **1994**, *23*, 221–236. [[CrossRef](#)]
55. Owen, J.S. A Survey of Unstructured Mesh Generation Technology. In Proceedings of the 7th International Meshing Roundtable Conference., Dearborn, MI, USA, 26–28 October 1998; Volume 3, pp. 239–267.
56. Ansys. Available online: <https://www.ansys.com/ja-jp> (accessed on 10 August 2023).
57. Ujiie, Y.; Kato, T.; Sato, K.; Matsuoka, Y. Curvature entropy for curved profile generation. *Entropy* **2012**, *14*, 533–558. [[CrossRef](#)]
58. Free3D. Available online: <https://free3d.com/ja/> (accessed on 10 August 2023).
59. cgtrader. Available online: <https://www.cgtrader.com/> (accessed on 10 August 2023).
60. Laerhoven, H.; van der Zaag-Loonen, H.J.; Derkx, B.H.F. A comparison of Likert scale and visual analogue scales as response options in children's questionnaires. *Acta Paediatr* **2004**, *93*, 830–835. [[CrossRef](#)]
61. Helmut, L.; Jan, M.; Hideaki, K.; Raphael, R. Symmetry as an Inter-Cultural Feature Constituting Beauty: Implicit and Explicit Beauty Evaluation of Visual Symmetry in Japan. *Empir. Stud. Arts* **2023**. [[CrossRef](#)]
62. Wagemans, J.; Van Gool, L.; D'ydewalle, G. Orientational effects and component processes in symmetry detection. *Q. J. Exp. Psychol.* **1992**, *44*, 475–508. [[CrossRef](#)]
63. Barlow, H.B.; Reeves, B.C. The versatility and absolute efficiency of detecting mirror symmetry in random dot displays. *Vis. Res.* **1979**, *19*, 783–793. [[CrossRef](#)] [[PubMed](#)]
64. Surazhsky, T.; Magid, E.; Soldea, O.; Elber, G.; Rivlin, E. A comparison of gaussian and mean curvatures estimation methods on triangular meshes. *IEEE Int. Conf. Robot. Autom.* **2003**, *2003*, 1021–1026.

Disclaimer/Publisher's Note: The statements, opinions and data contained in all publications are solely those of the individual author(s) and contributor(s) and not of MDPI and/or the editor(s). MDPI and/or the editor(s) disclaim responsibility for any injury to people or property resulting from any ideas, methods, instructions or products referred to in the content.